Journal of Metals, Materials and Minerals, 37(1), e2639, 2027

Sustainable biochar production from pine needle waste by retort heating for value-added functional carbon materials

Arpita Roshni BEHERA[1], Prachi SINGHAL[1,*], and Sunita RATTAN[1]

[1] *Amity Institute of Applied Sciences, Amity University Uttar Pradesh, Noida, Uttar Pradesh, 201313, India*

***Corresponding author e-mail**: psinghal@amity.edu

Received date:
2 February 2026
Revised date:
24 June 2026
Accepted date:
29 September 2026

Keywords:
Pine needles;
Biomass;
Carbonization;
Biochar;
Graphitization

Abstract

Sustainable management of pine needles, as a major forest waste product, is a critical challenge due to their high flammability, potential to create fire and ability to restrict growth of other vegetations. One of the possible solutions to this challenge is to utilize pine needles to produce value added products following the concept of circular economy. The present work focuses on utilizing pine needle waste to produce biochar and biochar derived functional carbon materials. The attempt has been made to carbonize pine needles into biochar through pyrolysis at different temperatures of 300°C, 400°C, 550°C and 700°C. Top Lit Updraft and Retort kiln method has also been explored to achieve large-scale conversion rate. The produced biochar is characterized for morphological and structural characteristics through CHNSO elemental analysis, SEM, TEM, FTIR, Raman, XRD, EDAX and XPS. The characterization results show that pine needle biochar produced through retort heating method provides good degree of carbonization and aromatisation with significant polarity index widening the versatile applications of the material. The biochar thus produced can be activated or functionalised into a range of significant functional carbon materials such as activated biochar, nano biochar, graphitized biochar etc. Further, an attempt has been made to graphitize the biochar through chemical activation using $Fe(NO_3)_3$ followed by thermal treatment. The result shows that biochar has been successfully converted into graphitized biochar at quite low temperature i.e. <1000°C. Graphitized biochar produced exhibits crystalline aromatic structure with well-organized layers as evident by SEM, FTIR, XRD and Raman studies, and can serve as a source to derive costly graphene-based materials. This adopted pathway of making biochar, thus exhibits the potential to solve the problem associated with accumulation of pine needle waste, that can serve as an alternative precursor for the synthesis of value-added synthetic functional carbon materials applicable to wide range of specific applications including adsorbent or catalysts for water remediation, CO_2 sequestration, filler for polymer composites, electrode materials, energy storage, etc.

1. Introduction

Pine tree waste, a major category of forest biomass residue in hilly areas, is primarily made up of pine needles poses a significant challenge due to its highly inflammable residue that creates forest fire hazards. It has substantial global availability, such as Himalayan regions encompassing India, Mediterranean coastal regions of Spain and southern France in Europe etc. Pinus roxburghii, commonly known as chir pine, predominantly available in Himachal Pradesh and Uttarakhand regions of India, occupying nearly 16% of total forest regions of India and yields around 1.37 MT to 2.37 MT of pine needles annually. Pine needles, represents a lignocellulosic biomass containing cellulose (23.5% to 38.7%), hemicellulose (20.1% to 23.4%), and lignin (17.3% to 23.5%) with low moisture content along with high volatile resin content and acidic nature. During peak summers, the shredded dry pine needles form a thick layer of foliage on ground, causing recurring forest fires leading to disruption of local livelihoods, increased carbon emissions, biodiversity loss such as destruction of flora and fauna and soil degradation etc. Further, the accumulation of pine needle over years, exacerbated by slow decomposition due to the high lignin content suppresses growth of any kind of vegetation for livestock with devastating consequences for flora, fauna, and rural communities [1]. To avoid these hazards, pine needles are mostly being used at local level as a heat source, but to a limited extent. Disposal of forest biomass through conventional burning method is not eco-friendly as it produces greenhouse gases thus, adversely affecting the environment and its climatic conditions. Thus, extra efforts are required to solve the issue of pine needle trash.

Alternatively, Pine needle biomass, being a complex mixture of cellulose, hemicellulose and lignin, could serve as alternative source to produce carbonaceous materials such as biochar, functionalized carbon, activated carbon, graphitized carbon etc. This fascinating class of carbon materials with exceptional physiochemical properties, has attracted tremendous industrial and research attention in the wide range of fields including adsorption, composite formation, energy storage, fuel cells, catalysis, etc. Thus, utilizing pine needles to produce carbon materials, as an alternative to conventional resources can potentially address unsustainable resource consumption, reduce fossil

fuels dependency, mitigate carbon emissions, and lower the risk of devastating forest fires caused by accumulated dry pine needles.

Biochar is a carbonaceous material, derived through pyrolysis of biomass, shows versatile applications in the field of soil amendment, carbon sequestration, environmental remediation, composite formation, applications in industries and even for energy production etc. Biochar exhibits advantages including good porosity, high surface area with active functional groups, good mechanical strength, thermal efficiency, easy handling and storage [1]. Its specific industrial applications such as industrial waste-water treatment, reinforcements in polymer composites (to achieve enhanced electrical and thermal properties), electrode preparation (for enhancing catalytic activity) helps in environmental management by solid waste valorisation making it an important tool for sustainable development [2–5]. Biochar, in its raw form or functionalised form is widely recognized as an efficient as well as sustainable filler in polymer composites, by acting as a potential low-cost substitute to conventional high-cost fillers like carbon nanotube, carbon black etc [6–9]. It reduces the carbon footprint of the polymer composites owing to its renewability, customization potential and ecofriendly nature [8].

Further, Biochar shows a great potential to synthesize a range of functional carbon materials including activated carbon materials, nano biochar, graphitized carbon, graphene, CNTs etc. due to its easily tuneable surface and porosity. Surface of the biochar could be tuned and activated through functionalisation (oxidation, sulphonation, amination etc.), doping with metal nanoparticles, grafting, thermal treatment etc. Further, biochar could be a sustainable resource for producing graphitized carbon and costly graphene-based materials. Biochar, being a complex material can be converted into graphitic structure synthetically at temperature above 1500°C. Synthetic graphite substitutes natural graphite as a high-performance material, finds significant industrial applications such as in Lithium-Ion batteries, semiconductors & electronic industries, high temperature furnaces, as electrodes, as refractory materials etc [2,10,11]. Synthetic graphite commercial production method relies on petroleum resources involving extreme temperature processing conditions with considerable environmental effects [12]. With increasing demand for synthetic graphite to match current demands of sustainable energy production and storage systems, efficient production methods with reduced environmental effect are increasingly focused. Alternatively, waste biomass (pine needles) derived biochar falls under sustainable resource category for synthesizing graphitized carbon with great potential. Further, formation of graphitized carbon could prove to be a key step towards sustainable production of graphene with wide range of important industrial applications in electronics field including electrode material for batteries, printable ink, etc. Graphitized carbon could be a probable resource for producing graphene-based materials through liquid phase exfoliation [13,14]. Graphene is a versatile material with 2D honeycomb lattice structure with high surface area and outstanding mechanical, thermal and electrical properties.

In this way, utilizing pine needles, a massive forest waste as feedstock to its maximum potential as a renewable and sustainable source for production of biochar and its derivatives using efficient as well as cost-effective thermochemical conversion processes such as pyrolysis lowers environmental impact by fostering carbon neutrality. Pyrolysis is an attractive option for the utilizing biomass to yield biochar [15].

The process of producing biochar through pyrolysis primarily involves heating biomass in limited oxygen environment, called as carbonization. Typically, carbonization is carried out in specialized kilns or furnaces at an operating temperature above 400°C. Studies shows that slow pyrolysis at low temperatures favour higher yield of biochar [16]. Kilns for scaled-up production of biochar depending on the need can be of different types such as Top-Lit Updraft (TLUD) kilns, earth-mound kilns, Retort kilns, Continuous pyrolysis kilns, etc. [16–19]. In this present study, the retort and top lit updraft technology was adopted to obtain high-quality biochar with optimized yield. Properties of biochar obtained through pyrolysis can be optimized varying the processing temperature as per its efficacy to the targeted application [15].

Such valorisation not only address the hazards posed by pine waste accumulation but also offers scope for resource recovery, renewable energy generation, environmental conservation, improved rural livelihoods thereby promoting circular bioeconomy goals in vulnerable mountainous regions. Thus, its useful applications, especially in the production of value-added products, demand further research. The research in the field of sustainable utilisation of pine needle waste to produce of biochar, derived carbon materials and their probable applications is still limited with many technical and scientific challenges. The present work thus focusses on exploring the utilization of pine needle forest waste as biomass to produce biochar and biochar derived functionalised carbon materials such as graphitic carbon materials in a sustainable manner using a simple retort kiln heating method, revealing the underlying mechanisms of thermochemical conversion from biochar to graphene-based materials. The main objective of the work includes in-depth comparative study of biochar produced in different method, analysing the physiochemical properties of the pine needle derived biochar, observing the effect of carbonization temperature and exploring the possibility of utilizing biochar as precursor to value-added functional synthetic carbon materials.

2. Materials and methods

2.1 Materials

Pine needles were collected from the forest area of Himachal Pradesh and were used as such without any pretreatment. Top Lit Updraft and retort kiln was procured from EcoPro, Auroville, India. Ferric nitrate [$Fe(NO_3)_3$] (98% purity), HCl (12M) were purchased from Qualigens and used as received.

2.2 Preparation of biochar from pine needles in electric furnace

The dry pine needle biomass was chopped into small pieces, and the biochar was prepared in a temperature-controlled electric furnace through slow pyrolysis in restricted supply of oxygen. All pyrolysis experiments were performed in triplicate (n=3), and the results are reported as SE (standard error). The pyrolysis temperature was increased at a rate of $5°C \cdot min^{-1}$ until the required temperature was reached. The chopped biomass was pyrolyzed for 2 h at different temperatures i.e. 300°C, 400°C, 550°C and 700°C and further labelled as CH_300, CH_400, CH_550, CH_700 respectively. After cooling, the biochar

was subjected to grinding to obtain coarse powder. The biochar samples were further weighed, and the yield (% biochar) was calculated.

2.3 Preparation of biochar from pine needles using top lit updraft (TLUD) and retort kiln method

To produce biochar, Pine needles were chopped and dried at 120°C followed by the two different routes as given below:

For production of biochar, Top Lit Updraft (TLUD) gasifier was used, which works in a temperature range of around 400°C [1]. The waste pine needles were treated in TLUD for approximately 2 h with a limited supply of oxygen as shown in Figure 1. The biochar produced are named as CH_TLUD.

For better carbonization of Biochar, retort heating methods was used in which pine needles were carbonized in a retort kiln for 2 h in a limited supply of oxygen as shown in Figure 1 [5]. The biochar thus produced is named as CH_retort.

The biochar obtained was grounded and sieved to get homogenized powder and kept in airtight container for further use.

2.4 Preparation of graphitized biochar through catalytic pyrolysis

The biochar obtained through retort heating was used for graphitization as shown in Figure 2. Approximately 15 g of biochar and about 24.23 g of iron nitrate [$Fe(NO_3)_3$] were used keeping the ratio of pure iron to biochar to approximately 22.4 by weight. Iron nitrate was dissolved in distilled water, resulting in formation of [$Fe(NO_3)3.9(H_2O)$]

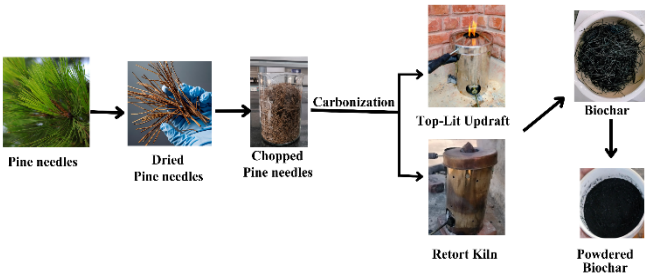


Figure 1. Schematic representation of formation of biochar through TLUD and retort kiln.

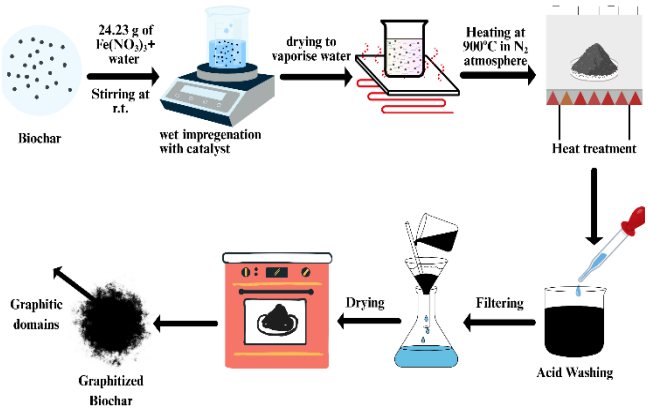


Figure 2. Schematic representation of Fe $(NO_3)_3$ mediated catalytic graphitization of biochar.

followed by the addition of biochar. The solution was stirred at room temperature for 3 h using solution impregnation method. The mixture was then kept for drying in a hot air oven at 90°C for 3 h to vaporize the water in the solution leading to formation of in a solid powder containing evenly distributed iron nitrate in biochar. The mixture was then placed in a silica crucible and treated at 950°C in nitrogen atmosphere in a tube furnace. The sample obtained was then washed several times with HCl solution and distilled water. In order to remove the iron, the biochar obtained was washed with approx. 200 mL 1 N HCl solution for about 45 min in an ultrasonic bath to break the carbon layer surrounding the iron particle. The reaction of Fe with HCl is provided in Equation (1) below.

$$Fe + HCl \rightarrow H_2 + FeCl_2 \quad (1)$$

The sample was then filtered. To check the presence of iron, Potassium hydroxide [KOH] was added to the filtered liquid. If the filtered liquid contains iron the solution turns green/ yellow colour due to reaction between $FeCl_2$ and KOH as given below in Equation (2), and no colour change was observed otherwise. The acid wash was repeated until the filtered solution has no iron particle marked by filtered liquid with transparent appearance. The powdered sample was then oven dried for 3 h to obtain the desired product [20].

$$FeCl_2 + 2KOH \rightarrow Fe(OH)_2 + 2KCl \quad (2)$$

2.5 Modification of biochar by metal oxide and preparation of electrodes

Biochar obtained from carbonization in retort kiln was activated using a metal oxide through hydrothermal synthesis method [21]. The synthesized metal oxide modified biochar (MO_retort) and CH_retort is used as a working electrode material to study electrochemical oxidation of paracetamol. For the preparation of working electrode, homogenous suspension of CH_retort and MO_retort were made by dispersing 3.35 mg of prepared catalyst along with Nafion (30 µL) in isopropanol (90 µL) through ultrasonication for 30 min. The obtained slurry was coated on a carbon paper followed by drying of the electrodes overnight at room temperature.

2.6 Characterization of biochar

The biochar prepared is characterized for detailed structural, morphological and chemical properties using various analytical techniques.

2.6.1 Yield of biochar

The yield of biochar can be determined by the ratio of the mass of biochar to the mass of biomass feedstock [19]. Studies have shown that there is decline in biochar yield with increase in temperature above 350°C [22]. The biochar Yield (%) is influenced by operating conditions like the temperature, heating rate, residence time and use of catalyst. Lower pyrolysis temperature at slow heating rate with increasing the residence time yields in greater amount of biochar [23]. The

percentage biochar yield was determined using the equation as given below [24]. Each pyrolysis experiment was performed in triplicates and the yield is presented as M±SE.

$$\text{Yield (\%)} = \frac{\text{mass of biochar}}{\text{mass of feedstock}} \times 100$$

2.6.2 CHNSO elemental analysis

The physicochemical properties and functional effectiveness of the biochar for various applications was analysed using CHNS analyser, an analytic functional testing UNICUBE to investigate elemental composition. Elemental analysis primarily involves investigating and measuring the elemental composition of elements such as carbon (C), oxygen (O), nitrogen (N), hydrogen (H), sulphur (S), and other trace elements. The H/C ratio provides information about the degree of carbonization as well as aromaticity of the biochar along with predicting the molecular structure of the aromatic cluster [25]. O/C serves as a stability index to assess the degree of oxidation of biochar as well as measure polarity of biochar [26]. The (O+N)/C ratio provides information about surface polar functional groups and the overall heteroatom content relative to carbon. The percentage of C, H, N, S, O elements are reported as M±SE (n = 3).

2.6.3 Morphological and textural studies

Scanning electron microscopy (SEM): The microscopic surface topography of biochar was studied using JEOL JSM-6610LV SEM which provides information about the change in surface roughness and physical structure post pyrolysis which is critical to targeted application. The change in morphology after pyrolysis helps in the optimization of pyrolysis condition and the feedstock type more desirable for the specific purpose. SEM coupled with energy dispersive X-ray analysis (EDAX) can be a helpful tool for elemental mapping to analyse the elemental distribution on biochar surface.

Transmission electron Microscopy (TEM): TEM provides detailed information at nano and atomic level revealing the crystalline domains, graphitic layers and arrangement of graphitic layers. The crystalline and graphitic domains provide information related to stability and thermal reactivity along with electrical conductivity.

Brunauer-Emmett-Teller (BET) Analysis: The textural and surface properties such as N_2 adsoprtion-desorption, pore size and pore distribution of biochar was analysed using BELSORP-maxII (BELSORP-series), Microtrac BEL Corp. The sample was degassed at 300°C for 3 h prior to BET analysis. The BET analysis was carried out at –196°C in nitrogen atmosphere. The pore diameter and pore size distribution was analysed from the N_2 adsorption-desorption isotherm and NL-DFT method is provided in Figure S3 (supplementary information). The BET of CH_700 and CH_retort has been briefly discussed in supplementary information (section 3).

2.6.4 Spectral studies

Fourier Transform Infra-Red Spectroscopy (FTIR): FTIR spectra provides information regarding the surface functional groups of biochar. The prepared biochar was analyzed using Nicolet iS50 FTIR spectrometer in the range of 4000 cm^{-1} to 400 cm^{-1} wave number.

Raman Spectroscopy: Raman spectroscopic study of the biochar samples was carried out using HORIBA JOBIN VYON, LabRam HR- MNCF 031 with laser power of 15 mW, in the range of 500 cm^{-1} to 3500 cm^{-1}. The information depth and wavelength at which the analysis was carried out was 50 nm and 514 nm respectively.

X-ray Diffraction (XRD): XRD involves measuring scattering of X-rays when it interacts biochar. It provides information about the crystalline phases by distinguishing between amorphous and crystalline regions. It also provides relation between temperature profile and development of turbostatic and graphitic carbons. XRD was performed at scan rate of $2°\cdot min^{-1}$ in the range of 5° to 80°.

X-ray Photoelectron Spectroscopy (XPS): XPS involves irradiating outer surface of biochar with X-rays leading to photoelectron emission whose energy gives information about the elemental composition along with the chemical states of atoms present on the outer surface. It identifies the relative abundance of elements along with their characteristic binding energies.

2.6.5 Electrochemical measurements

A potentiostat PGSTAT 302N (Metrohm) controlled by Nova software was used for electrochemical assays. The electrochemical evaluation of CH_retort and MO_retort electrode was performed in a three-electrode system using the biochar-based material as working electrode, Ag/AgCl as reference electrode and Pt wire as counter electrode. The electrochemical performance of CH_retort and MO_retort electrode material towards paracetamol was evaluated by using cyclic voltammetry. The cyclic voltametric measurements were performed in triplicates. Cyclic voltammetry was carried out both in absence (blank) and presence of 0.001 M paracetamol at a scan rate of 50 $mV\cdot s^{-1}$ using 0.1 M phosphate buffer solution (pH–7) as supporting electrolyte.

3. Result and discussion

Top-lit updraft (TLUD) micro-gasifiers aids in conversion of biomass into biochar and combustible gases through a controlled pyrolysis process. The formation of char is achieved by limiting oxygen supply to the lower reactor, thus preventing further oxidation [27]. Dry biomass is loaded into the inner chamber and ignited with fuel at the uppermost layer, resulting in a downward-propagating migratory pyrolytic front. As the migratory pyrolytic front propagates, thermal decomposition of feedstock occurs without required amount of oxygen, thus leading to biochar formation along with volatile organic compounds, and volatile gases such as CO, H_2 and CH_4 [28]. The upward movement of combustible gas is facilitated by the natural draft created by the difference in density between the hot gases and cooler air. This draft helps in creating a steady supply of primary air from the bottom of the reactor, which is useful for partial oxidation and sustaining various endothermic pyrolysis reactions. The secondary air enters from the top of the fuel bed, where it mixes with the evolved pyrolytic gases, resulting in a high-temperature combustion zone promoting the oxidation of volatile species, thereby producing a clean carbonization with minimal particulate emissions. The double-walled TLUD minimizes thermal

loss and preheat the incoming secondary air, further leading to the enhancement of gas-phase combustion and overall thermal profile of the reactor. The fixed-bed aids in the gradual reduction in fuel volume as pyrolysis progresses, with the residual biochar accumulating above the advancing migratory pyrolytic front [28]. This technology plays a key role in sustainable energy generation, climate change mitigation and development of circular economy [29].

Retort kiln typically has a closed cylindrical carbonization chamber, where the biomass feedstock is isolated from direct combustion [29]. It consists of two concentric cylindrical chambers. The outer chamber is used as a combustion chamber where the fuel is burned to produce flue gases which further recirculates to improve the thermal efficiency by re-combusting the volatile gases and thereby providing continuous heat for the carbonization process. The outer cylindrical chamber has several holes at the bottom to allow natural convection of air required for the combustion of fuel in the combustion chamber. The volatile gaseous products escape into air from the chimney present at the top of the reactor. The feedstock is placed in the interior chamber within the reactor. Pre-dried biomass is required for sustained pyrolysis and high-quality biochar yield [30]. Retort kiln design enhances operational efficiency as well as the product quality [31]. It has been reported that a range of biomass feedstock such as oil palm fibre, sugarcane bagasse and various fruit waste have been successfully converted to biochar using retort kiln with more than 40% yield. Thus, retort kiln provides an energy efficient as well as a scalable solution for product development and climate mitigation [29].

3.1 Characterization of biochar

3.1.1 Yield of biochar

It was found that the yield of biochar was affected by processing parameters such as temperature, carbonization method. The biochar yield ranges from 70.37 ± 2.91% to 30 ± 1.51% and as the carbonization temperature increases, the biochar yield progressively decreases as mentioned in Table 1. Biochar obtained by retort heating method has an optimum yield of 45.7 ± 1.95% without compromising the quality of biochar.

3.1.2 Elemental analysis of biochar

Biochar could be a reasonable substitute to replace synthetic and expensive carbon-based material in different applications with comparable physical & chemical properties. The physio-chemical properties of biochar depend on its structure, chemical composition and surface characteristics that in turn varies with the biomass type, temperature and other process conditions, and thus can be tailored and applied for different possible applications. Elemental analysis could provide potential insight into the characterization of the prepared biochar with respect to its composition, structure and surface functionality, which is directly linked to the performance of biochar that could include sequestration of carbon, soil amendment, water remediation, composite formation, energy storage materials [32,33].

Elemental analysis of biochar provides the quantitative measurement of C, H, N, S, O elements present in biochar that is often used to calculate key elemental ratios including H/C, O/C, C/N and (O+N)/C ratios. The H/C ratio reflects the carbonization degree and aromaticity of biochar. Biochar with stabilized carbon can effectively be applied to soil as amendment to enhance the soil properties such as cation exchange capacity, pH, water holding capacity and availability of nutrients etc. [34].

O/C is commonly taken as a stability index that evaluates degree of oxidation of the biochar as well as measures polarity of biochar [26]. The (O+N)/C ratio provides information about surface polar functional groups and the overall heteroatom content relative to carbon. Biochar with higher O/C ratio and higher polarity may act as better adsorbent for removal of polar pollutants through electrostatic interactions. Even aromatic character in biochar may influence non-covalent interactions between biochar and the delocalized electrons of the pollutants during adsorption process. Aromaticity in biochar may further get affected by the presence of oxygen functionalities with specific electron donating or withdrawing behaviour [35]. The nitrogen containing functionalities control surface polarity and acidic or basic nature. The elemental composition of pine–needle biochar samples (CH_300, CH_400, CH_550, CH_700) prepared in temperature-controlled furnace in inert atmosphere at temperatures 300°C, 400°C, 550°C and 700°C respectively along with pine needle biochar (CH_retort) prepared in retort kiln is summarised in Table 2. The table summarizes the elemental compositions (C, N, H, S, O) and derived atomic ratios including H/C, C/N, O/C, (O+N)/C ratios. The result shows that with the increase in pyrolysis temperature, the carbon content increases from 58.63% C for CH_300 to 72.31% C for CH_700, the possible reason may be devolatilization of oxygen and hydrogen rich volatiles at higher temperature (supported by TGA of Pine needles given in Figure S1. (Supplementary material) [36]. Devolatilization of oxygen and hydrogen occurs fundamentally through dehydration,

Table 1 Biochar yield at various pyrolysis temperatures (300°C, 400°C, 550°C, 700°C) and biochar yield of retort biochar (M±SE, n=3).

Char type	CH_300	CH_400	CH_550	CH_700	CH_Retort
Yield (%)	70.37 ± 2.91	66.26 ± 2.77	41.66 ± 2.01	30 ± 1.51	45.7 ± 1.95

Table 2 Elemental composition of biochar samples (M±SE, n=3).

Char type	C [%]	N [%]	H [%]	S [%]	O [%]	H/C ratio	C/N ratio	O/C ratio	(O+N)/C
CH_300	58.63 ± 1.03	2.33 ± 0.042	5.524 ± 0.1	0.256 ± 0.01	28.033 ± 0.5	0.094	25.163	0.478	0.517
CH_400	68.32 ± 1.16	2.74 ± 0.08	4.19 ± 0.09	0.083 ± 0.005	18.482 ± 0.4	0.061	24.955	0.270	0.310
CH_550	71.73 ± 1.28	2.5 ± 0.065	3.035 ± 0.04	0.045 ± 0.003	14.727 ± 0.2	0.042	28.701	0.205	0.240
CH_700	72.31 ± 1.39	2.5 ± 0.061	3.279 ± 0.08	0 ± 0.001	11.186 ± 0.15	0.045	28.947	0.154	0.189
CH_retort	70.23 ± 1.26	2.48 ± 0.056	3.095 ± 0.06	0.049 ± 0.004	15.014 ± 0.28	0.044	28.318	0.213	0.249

deoxygenation and carbonization phenomenon, leading to higher C% such as for CH_700 with simultaneous lowering of H/C and O/C ratio to 0.045 and 0.155 respectively. N and S content remains fairly stable throughout showing minimal loss during carbonization. Low molar O/C ratio was found to decrease significantly due to loss of oxygen functionalities making the biochar more hydrophobic. Result indicates higher aromaticity and structural stability of CH_700 due to effective carbonization, however, less surface functionality owing to reduced oxygen functionalities. makes it best suited for applications such as carbon sequestration and soil amendment etc. [37].

Elemental composition of pine needle biochar prepared through retort kiln method (CH_retort) is compared with biochar prepared in the furnace. Elemental analysis result reveals that carbon content of CH_retort is comparable to that of biochar; produced at 700°C (CH_700) in tube furnace. The similar H/C ratios of CH_retort and CH_700 indicate carbonization mediated condensation and aromatization enhancing stability of the biochar. Pyrolysis through retort kiln method is considered as one of the most efficient pyrolysis methods for preparation of biochar because it uses the strategy of re-combusting flue gas to generate more thermal energy for improved carbonization [29]. However, CH_retort with O% (15.014), O/C ratio (0.21) and (O+N)/C ratio (0.249) is comparable to that of CH_550 revealing moderate polarity and presence of oxygen functionalities in the CH_retort biochar. The oxygen functionalities on biochar surface are responsible for providing functional adsorption and electroactive sites that makes biochar promising for adsorption, catalysis, water remediation, and capacitive applications [38]. The result shows that retort kiln process provides highly carbonised biochar, indicating high degree of aromatisation, along with retention of active surface functional groups on biochar as indicated by polarity index.

3.1.3 SEM and EDAX of biochar

The microscopic surface morphology of biochar CH_550, CH_TLUD and CH_retort was studied using SEM to study the effect of carbonization methods on morphological evolution of the biochar surface as shown in Figure 3. The EDAX of CH_TLUD, CH_retort is given in Figure S2. (Supplementary material) which provides information about elemental mapping to analyse distribution of elements on biochar surface [39–42]. The surface morphology and physical properties like porosity of material, arrangement of pores etc. are studied using SEM. For biochar this is critical as the properties required for various applications such as filtration, soil enhancement etc. are very much influenced by its structural arrangement as well as physical properties such as pore distribution, uniformity and pore volume etc. It was observed that SEM images of all the biochar samples displayed a rough, irregular and structurally complex surface with several pores of various sizes. The porous morphology might be due to retention of natural porosity of the precursor or rapid emission of volatiles during carbonization leading to formation of new pores [43]. The surface features observed were formed probably due to breakdown of cellulose, hemicellulose components and loss of volatile substances during gasification that results in non-uniform growth while cooling [44–46]. It can be observed that CH_550 has less porosity when compared to CH_TLUD and CH_retort. CH_550 has

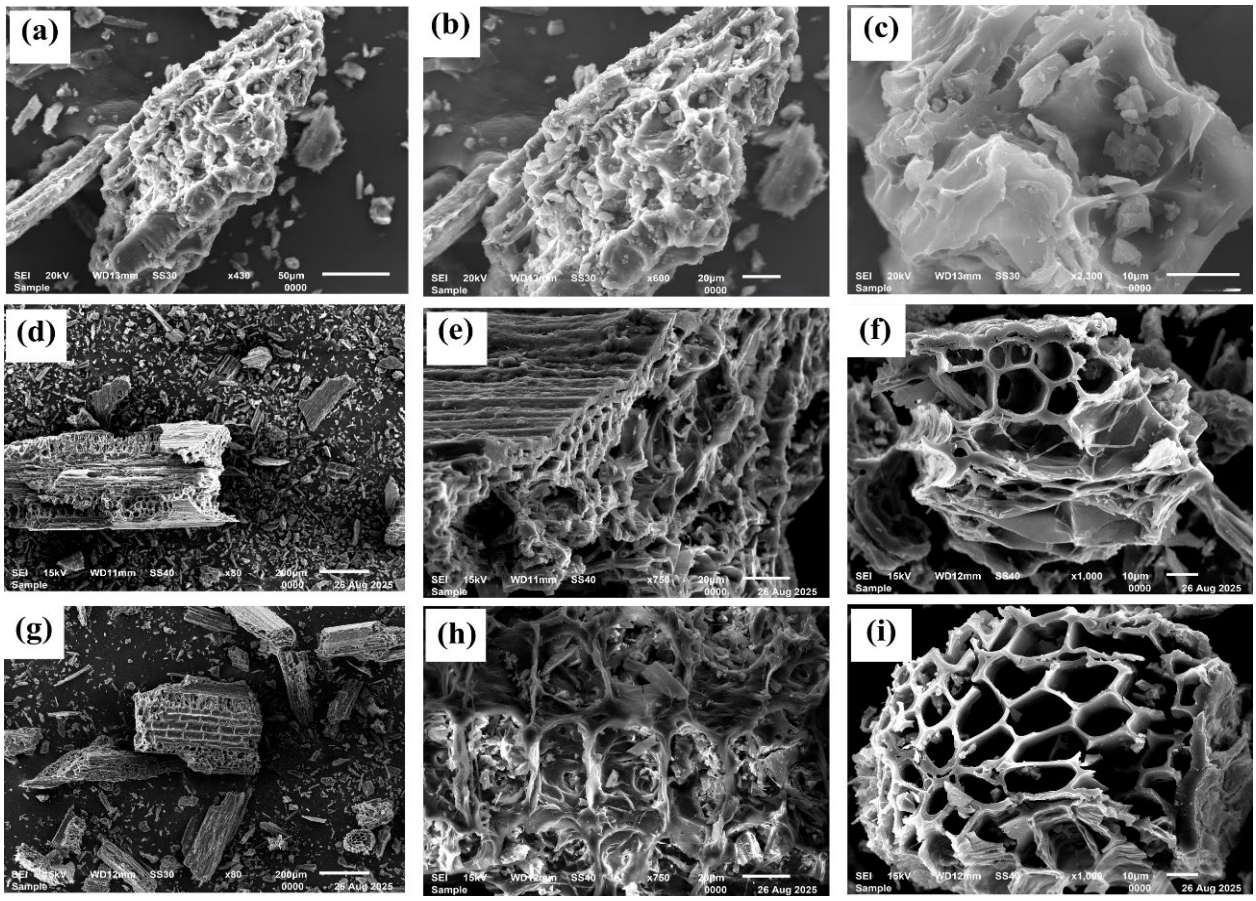


Figure 3. SEM images of (a–c) CH_550, (d–f) CH_TLUD, (g–i) CH_retort biochar.

fewer pores with irregular arrangement, and a significant number of pores were observed to be blocked might be due to the presence of contaminants such as tar and ash produced during the carbonization process [47]. CH_TLUD produced by slow pyrolysis is expected to demonstrate well defined porous structure with preservation of cellular structures such as long, tubular vessels and honeycomb pattern. The surface of CH_TLUD biochar has uniform well developed open mesopores and micropores formed as a result of escape of volatile gases during pyrolysis. The carbonization process cleans up the structure by removing tars and increasing size of the pores [48]. CH_retort involves carbonization in an oxygen limited; sealed container and often volatile gases are recirculated for effective charring and tar cracking. This typically leads to formation of more consistent and extensive network of pores with thinner walls as depicted in the SEM images.

3.1.4 FTIR of biochar

The FTIR comparison powerfully illustrates that pyrolysis temperature is the primary driver of the structural change on the surface of biochar. The FTIR spectra of CH_300, CH_400, CH_550, CH_700, CH_TLUD and CH_retort provide information about the functional groups present on the surface of biochar as shown in Figure 4(a). As we move from low-temperature (CH_300) to high-temperature (CH_700) biochars, the spectra show clear and consistent evolution of chemical structure due to increase in carbonization and aromatic condensation. This is evidenced by the decrease and eventual loss of O–H and aliphatic C–H groups, strengthening of the aromatic C=C backbone and the simplification and loss of complex C–O functionalities through dehydration, decarboxylation, and decarbonylation reactions showing volatile matter and aliphatic side chains are being cleaved and lost [49]. The disappearance of the C–H peaks indicates the cracking and loss of aliphatic side chains from lignin and cellulose. This trend aligns with the known thermochemical transformation of biomass, where volatile, oxygen-rich compounds are lost first, followed by the growth and ordering of polycyclic aromatic graphene-like sheets [50]. As other functionalities vanish, this backbone structure becomes the primary feature of the biochar. The residual oxygen is likely incorporated into very stable heterocyclic structures or persistent quinone groups, rather than the labile functional groups found in low-temperature chars. Lower temperature biochars (CH_300, CH_400) are rich in oxygenated functional groups, making them more hydrophilic and reactive, which is desirable for applications like soil amendment and cation retention [51]. Biochars (CH_550, CH_700, CH_retort) are more condensed, aromatic, and carbonaceous, with improved stability and high surface area, suitable for carbon sequestration or contaminant sorption via pore-filling and π-π interactions. CH_300 exhibits a strong broad peak at ~3400 cm^{-1} corresponding to O–H Stretch indicates a high concentration of moisture, alcohols, phenols, and carboxylic acids [52]. As the temperature of pyrolysis is increased, the intensity of O–H stretch gradually decreases as the population of hydrogen-bonded O–H groups is greatly diminished. There are some prominent sharp peaks in CH_300 in the range of ~2900 cm^{-1} to 2800 cm^{-1} (C–H Stretch) which shows a significant presence of aliphatic chains [53]. As the temperature is increased to 700°C, the intensity of C–H stretches noticeably reduced indicating complete pyrolysis of most aliphatic structures. The broad peak around (~1600 cm^{-1} to 1700 cm^{-1}) suggests a mixture of aromatic C=C (1585 cm^{-1} to 1600 cm^{-1}) and carboxylic C=O (1665 cm^{-1} to 1760 cm^{-1}) present in CH_300. With the increase in carbonization temperature, the peak at ~1600 cm^{-1} becomes more distinct, suggesting a relative increase in aromatic C=C as some oxygenated groups decompose thus, becoming a dominant feature of aromatic region [56–59]. This can be further confirmed from the increased intensity of out of plane deformation of aromatic C–H at 875 cm^{-1} in CH_550, CH_700, CH_TLUD, CH_retort [58]. Similarly, the carboxylic C=O shoulder at 1705 cm^{-1} is much less pronounced, and the broad band of C–O has decreased substantially in intensity indicating most labile oxygen-containing groups (like acids and alcohols) have been decomposed. A band of few small peaks in the region of 1300 cm^{-1} to 1000 cm^{-1} represents a rich diversity of alcohols, phenols, ethers and carboxylic acids in CH_300 has now disappeared. The intensity of the peak at 1030 cm^{-1} representing carbon of undecomposed cellulosic and lignin component reduces evidently as the temperature is increased. In CH_300 and CH_400 the peaks at 1448 cm^{-1} and 1385 cm^{-1} accounts for the C=O stretching of ketones and O–H bending of phenols of the lignin components respectively whereas the bands at around 1160 cm^{-1} and 1270 cm^{-1} corresponds to C–O stretch of pyranone rings and guaiacyl monomers of the cellulosic components. This indicates CH_300 is the least carbonized closely resembling the original biomass, retaining most of its oxygenated and aliphatic functional groups. However, the increased intensity of C–H out-of-plane stretch around 875 cm^{-1} in CH_550 indicates greater degree of condensation where smaller aromatic units condense to from larger sheets. It can be stated that dehydration of lignocellulosic components starts at 300°C which is followed by improved degree of condensation and aromatization at 550°C and so on [59].

CH_TLUD profile falls between CH_550 and CH_700. It shows a very weak O–H stretch, no C–H stretch, a strong aromatic C=C peak, and a weak C–O band. This indicates a higher degree of carbonization, similar to the 550°C to 700°C range, which is consistent with the high temperatures achievable in TLUD reactors. However, O–H peak in CH_retort is absent indicating almost all O–H functional groups have been eliminated. Disappearance of C–H Stretch shows reduced intensity of detectable aliphatic structures. A distinct peak at ~1600 cm^{-1} is purely due to aromatic C=C stretch [60]. The lack of a C=O shoulder suggests loss of carboxylic acids, which is only present in TLUD and CH_300 at 1705 cm^{-1}. C–O Stretch broad band is very weak, indicating that most ether, ester, and phenolic C–O linkages have been broken [61]. All these phenomena demonstrate highly carbonized, condensed aromatic structures in CH_550 and CH_retort whose surface is largely deoxygenated and chemically inert compared to the lower-temperature chars.

3.1.5 Raman spectroscopy of biochar

Raman spectroscopic studies were used to analyze the changes in microstructure of biomass, when treated under varying range of pyrolytic temperature, that results in the thermal moulding of carbon domains and attaining specific structure of biochar. It has been reported that thermal treatment results in carbonization and aromatization with development of disordered graphitic domains at high temperature

during biochar formation. In visible Raman spectra of CH_550 and CH_retort biochar as represented in Figure 4(b), two predominant bands D band (1340 cm^{-1}) and G band (1570 cm^{-1}), corresponding to disordered graphitic domains and sp^2– hybridized ordered, carbon domains, respectively can be observed. Some other less dominant, D1 (1342 cm^{-1}), D4 (1110 cm^{-1}) spectral bands can be observed that further represents the specific carbon structural features of biochar as summarized in Table 3.

Taking in reference, the Raman spectrum of single crystal graphite as reported in literature, where only G band (1585 cm^{-1}) is present, and in the spectrum of microcrystalline graphite, that exhibits an additional D band due to the presence of improperly stacked graphitic layers and disordered aromatic carbon domains [62]. D band is absent in defect free graphite because D band arises owing to defect activated Raman resonance. In contrast, the 2D band (2639 cm^{-1}), an overtone of D band, can be observed in defect free graphene. The D band around 1300 cm^{-1} to1350 cm^{-1} in carbon materials is related to defect induced band, arises due to out of plane movement of carbon atoms [12]. This band provide information about structural information such as presence of defects and symmetry of atoms present near the edge of graphitic layer when the graphite transitions become allowed. The stretching modes of sp^2 carbons gives rise to G band which occurs in the range of 1520 cm^{-1} to1620 cm^{-1} [62].

The Raman spectra as shown in Figure 4(b) of the pine needle CH_550 biochar is fitted into 3 peaks: a G band at around 1585 cm^{-1}, a D1 band at approximately 1342 cm^{-1}, D4 band at 1114 cm^{-1} and 2D band at around 2639 cm^{-1}. The D-Peak at 1342 cm^{-1} originates from non-crystalline, sp^3-hybridized carbon structures. Sharp G-band represents significant degree of graphitization, that indicates the transformation of amorphous carbon into ordered graphitic domains when pine needles are treated at temperature range of 550°C [63]. In the spectrum of CH_TLUD, the peaks are not well defined, identifying the material as still rich in sp^3 carbon domains with low order of aromatic domains. However, in the spectrum of CH_retort well–defined D, G and 2D bands, similar to CH_550 were observed. It can be observed that the intensity as well as sharpness of G and D bands are more in case of CH_550 when compared to CH_retort. Raman spectroscopy results are found to be in good agreement with the FTIR findings, indicating existence of aromatic clusters, confirming growth of graphitic domain of biochar due to thermal stress during carbonization. During pyrolysis, the transformation of amorphous carbon into ordered graphitic domains occurs as volatiles and condensates polymerize into larger aromatic clusters.

3.16 XRD of biochar

XRD analysis was performed for CH_300, CH_400, CH_550, CH_TLUD, and CH_retort. Figure 4(c) shows the XRD patterns of biochars obtained at different temperatures, depicting the patterns of the biochar samples with broad amorphous graphite peaks. The broadness of the peak talks about the amorphous nature of biochar produced. Such biochars are commonly known as turbostatic chars which is indicative of disordered graphitic crystallites [64].

The XRD results of CH_300, CH_400, CH_550 and CH_TLUD biochar reveal that the broad Peaks around 16° to 22° corresponding to (002) crystal plane which is indicative of crystalline cellulose as represented in Figure 4(c) [65]. As the carbonization temperature increases from 300°C to 550°C, the intensity of these two peaks decreases and becomes broader due to partial structural degradation of cellulose leading to reduced crystallinity [48,66]. It shows complete destruction of structure of biomass during char formation at temperatures above 400°C, [67]. Paris *et al.* has confirmed that the during the charring process, the complete decomposition of the skeletal composite structure is followed by the formation of aromatic structures [68]. Similar findings also have been reported for the carbonization of feedstocks such as Jatropha curcas, nutshell etc. [67,69]. The broad peak in the region 16° to 22° is mostly flattened in CH_retort as shown in Figure 4(c), which can be explained by the progressive and almost complete loss of

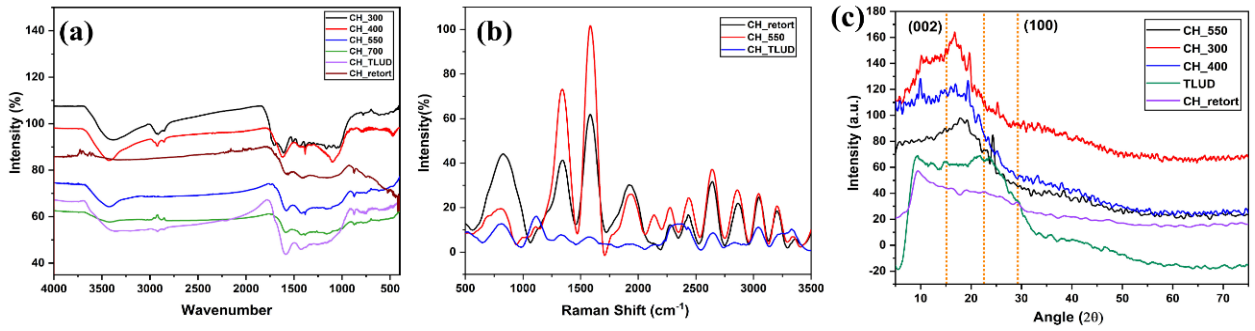


Figure 4. (a) FTIR spectra of CH_300, CH_400, CH_550, CH_TLUD, CH_retort, (b) Raman spectra CH_550, CH_retort, CH_TLUD, and (c) XRD of CH_300, CH_400, CH_550, CH_TLUD, CH_retort.

Table 3. Position of bands in Raman spectra of biochar samples.

Band name	Position of band in CH_retort [cm^{-1}]	Position of band in CH_550 [cm^{-1}]	Description
G	1585	1585	Stretching vibrations in aromatic rings of graphite
D1	1342	1342	Indicates in-plane defects in graphitic lattice due to defects and heteroatoms
D4	1114	1110	Shows presence of C=C and C–C bond or mixed sp^2–sp^3 bond or presence of structures like polyene at the periphery of crystallites
2D	2639	2643	Overtone of D band representing graphitic domains

crystallinity in cellulose. At the same time, there is a small but distinct peak around 26° (2θ) in CH_550 can be observed, corresponding to development of graphitic domains suggesting occurrence of crystallization at temperature 550°C. However, this small peak indicates higher structural order, which have not yet attained a complete crystalline structure [70]. This peak represents higher degree of orientation and occurs due to the parallel and azimuthal orientation of the carbonized lamellae 002 [71]. Also, a new peak is observed around 43° (2θ) in CH_550 which corresponds to condensed aromatic carbonized planes in the biochar. This peak at 43° corresponds to 100 plane depicting crystalline orientation of carbon which further indicates formation of turbostatic carbon crystallite, a transition towards more ordered arrangement of aromatic carbon [72–74]. This confirms formation of crystalline domain in the amorphous region in biochar owing to formation and successive development of atomic order in biochar, indicating simultaneous crystallization and increase in crystallize size [4,48]. However, lesser number of distinct peaks in CH_retort suggests the innate amorphous properties of the biochar sample [75]. In CH_retort a narrow peak around 29° (002 plane) indicates that the synthesized material predominantly contains disordered carbon lattices [76–78]. However, there was a significant reduction in the cellulose content in CH_retort evident from the reduced intensity of broader peak observed approximately around 16° to 22°, indicating simultaneous partial degradation of cellulosic material and development of atomic order within biochar which is more like a transition towards ordered arrangement of aromatic rings [79].

3.1.7 TEM of biochar

TEM micrographs of pine needle biochar (CH_retort) reflect discrete morphological evolution of biomass during pyrolysis as shown in Figure 5. The biochar particles predominantly exhibit thin, wrinkled, and sheet-like structures with irregular shapes (edges) due to oxidation process, characteristic of partially graphitized aromatic carbon domains formed through the thermal decomposition of lignocellulosic material [80,81]. The wrinkles and folds might be due to introduction of oxygen functional groups. These carbon layers are typically associated with higher pyrolysis temperatures, which promote increased aromaticity and partial structural ordering. Additionally, regions of high electron density visible as dark inclusions are attributed to the retained or thermally transformed inorganic constituents such as Mg, K, Ca, and Si [82]. These mineral phases are known to be naturally present in pine needles and can persist in the carbon matrix post-pyrolysis. The particle morphology appears heterogeneous, with sizes ranging from submicron fragments to nanoscale sheets. This broad distribution reflects the fragmentation of the biomass structure during carbonization. The contrast and textural variations suggest a combination of amorphous and microcrystalline carbon domains, consistent with prior findings on pine needle biochar produced at moderate to high temperatures [83].

3.1.8 XPS of biochar

XPS analysis provides information about the elemental composition, chemical state, and type of bonding present on the surface of the prepared biochar. The XPS spectra with both survey scan and narrow scan plots of detected elements in CH_retort are given in Figure 6(a) and Figure 6(b–h) respectively. The survey scan plot of CH_retort confirms presence of C, O, N, Ca, F and Mg elements on the surface. The presence of such elements in biochar provides an option to prepare multi-elemental doped carbon material.

In the deconvoluted spectra of C 1s (Figure 6(b)), the peak at 284.76 eV corresponds to graphitic carbon or aromatic carbons such as

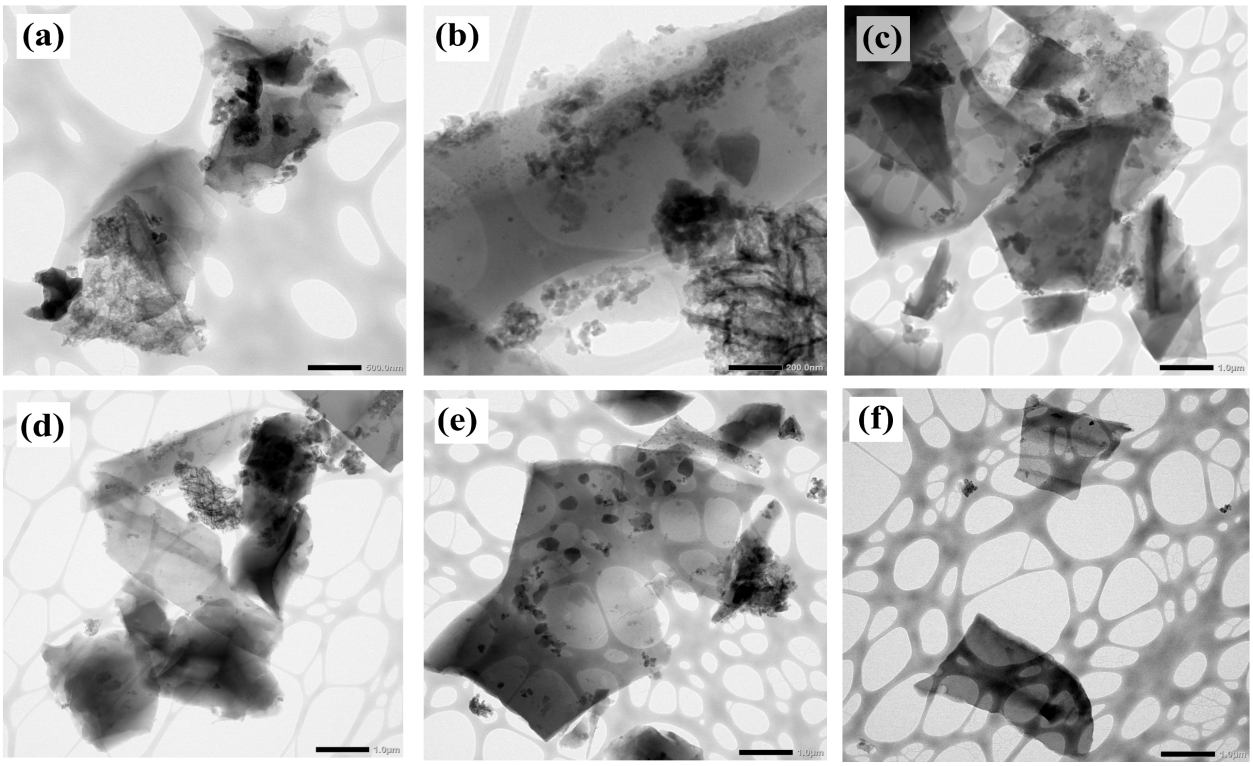


Figure 5. TEM images of CH_retort (a–f).

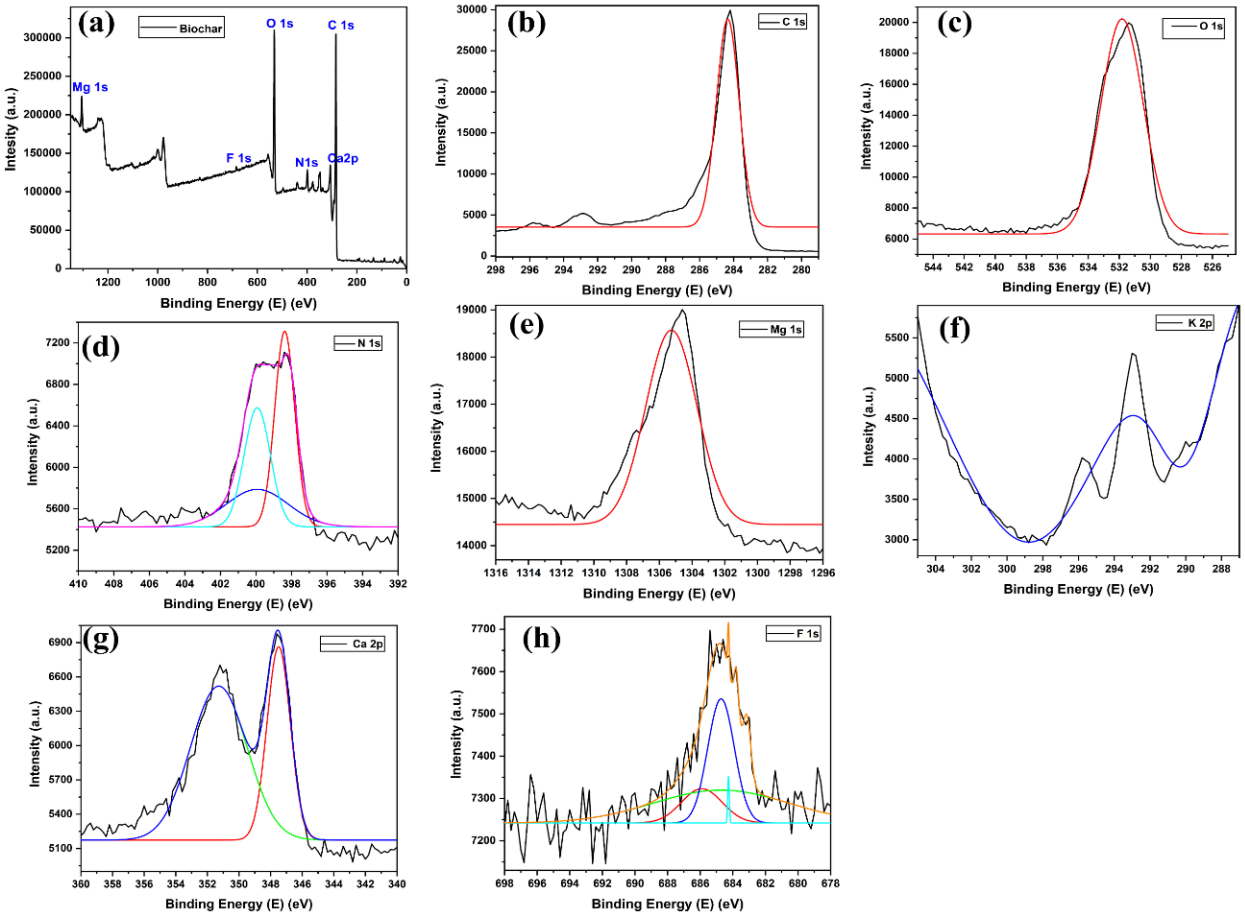


Figure 6. XPS of CH_retort (a) Survey Spectra of C, O, N, Mg, Ca, F of CH_retort biochar, (b) C 1s, (c) O 1s, (d) N 1s, (e) Mg 1s, (f) Ca 2p, (g) K 2p, and (h) F 1s.

C–C, C–H [72,73]. The deconvoluted N 1s spectrum (Figure 6(d)) exhibits three distinct peaks at 398.3 eV, 399.8 eV and 399.9 eV which correspond to pyridine-based nitrogen atoms, graphitic N and pyrrolic N respectively. Further, it indicates that the N atoms form bond within the carbon crystal lattice [73,84,85]. The deconvoluted O 1s narrow scan spectra show a peak at around 531.3 eV corresponding to C–O bond in phenols, carbonyl group, aromatic rings and ethers. The spectra of the Mg 1s produced only one peak at 1304.55 eV which could be possibly due to the Mg–O bond in MgO or $(Mg(OH))_2$ on the surface of CH_retort [84,86,87]. The high-resolution K 2p spectrum exhibits 2 peaks which corresponds to K $2p^{3/2}$ in the range of 292 eV to 295 eV and plasmons at 305 eV [88,89]. The Ca $2p^{1/2}$ can be deconvoluted into Ca–O corresponding to Ca $2p^{1/2}$ at around 351.21 eV and Ca $2p^{3/2}$ at around 347.42 eV respectively which is characteristics of calcite form [90,91]. F 1s XPS analysis shows four F 1s signals at around 684.26 eV, 684.72 eV, 684.5 eV and 685.92 eV respectively. The signal at 684.26 eV is assigned to hydrogen bonding (H–O–H···F), while the signal at around 685.92 eV is consistent with formation of FeF_3. In addition, the formation of NaF and N–Fe–F bonding might be responsible for the peak at 684.5 eV and 684.72 eV respectively [92].

3.2 Characterization of graphitized biochar

Biochar is further activated and thermally treated to convert it into graphitized biochar that could be a cost effective and sustainable path for producing functionalised carbon nanomaterials such as carbon nanotubes, carbon nanosheets and graphene-based materials, etc. To understand the potential of biochar as a cheaper and sustainable precursor for the production of synthetic carbon nanomaterials, it is essential to study the structural and functional properties such as surface properties, morphology, structural order, arrangement of graphitic domains, surface groups etc.

3.2.1 Mechanisms of catalytic graphitisation of biochar mediated by $Fe(NO_3)_3$

During catalytic graphitization, $Fe(NO_3)_3$ acts as a precursor for in situ generation of dispersed iron based nanoparticles, which further promote reorganization of amorphous carbon into graphitic layers at comparatively low temperature of 950°C through dissolution-precipitation mechanism [93]. This dissolution-precipitation mechanism helps in lowering the activation energy of graphitization, enabling formation of graphitic layer far below the conventional non-catalytic graphitisation temperature (>2500°C). As shown in Figure 7. $Fe(NO_3)_3$ first decomposes to Fe_2O_3 and Fe_3O_4, which are subsequently reduced by surrounding carbonaceous matrix and pyrolytic gases such as CO and H_2 leading to the formation of Fe_3C and metallic Fe nanoparticles [94]. Due to their nanoscale dimensions, the Fe_3C/Fe particles interact with the surrounding carbon matrix by providing abundant active sites for carbon dissolution. The dissolution of amorphous carbon atoms in

iron particles take place until a carbon saturated Fe–C phase is reached which is followed by diffusion through catalyst and reprecipitation as thermodynamically stable graphitic carbon. The repeated dissolution and reprecipitation cycles reorganize the disordered amorphous carbon structure, facilitating formation of stacked graphitic layers with increased crystallinity [95]. Simultaneously, the transient formation and decomposition of Fe_3C may further assist in carbon atom transport, bond rearrangement and ordering. This indicates that the carbide mediated rearrangement and dissolution-precipitation pathways operate concurrently depending on the chemical state as well as particle size of catalyst [96]. Studies show that early formation of Fe_3C is thermodynamically favoured when iron oxide is reduced carbo-thermally whereas the formation of same from metallic Fe only occurs at temperature above 820°C [97].

CH_retort biochar with large pores offer structural advantages such as effective catalyst infiltration through the larger transport pores. The improved infiltration of catalyst such as $Fe(NO_3)_3$ is beneficial during catalyst impregnation and subsequent catalytic graphitisation at comparatively low temperature, making CH_retort a very good precursor material for the production of graphitised carbon. The macropores promote uniform catalytic distribution during impregnation and aids in efficient carbon reorganization during graphitization.

3.2.2 SEM of graphitized biochar

Intriguingly, SEM images as represented in Figure 8, revealed significant structural changes for graphitized biochar in comparison to CH_retort. The graphitized biochar is well ordered, less porous with enhanced crystallinity, where graphene layers are stacked in layers. This arrangement of stacked graphene layers with some porosity is a key feature of graphite like carbonaceous materials [98].

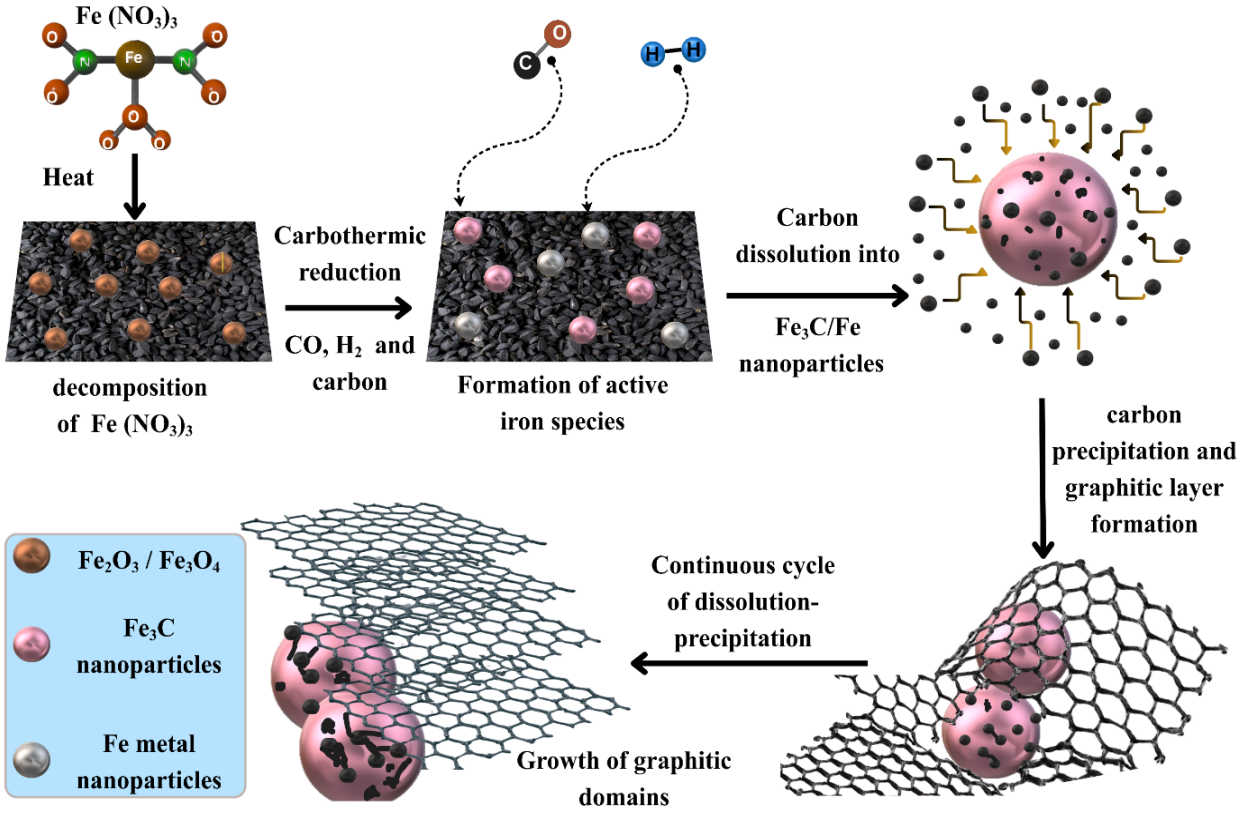


Figure 7. Schematic representation of mechanism of graphitic layer formation by Iron catalysed graphitization of biochar.

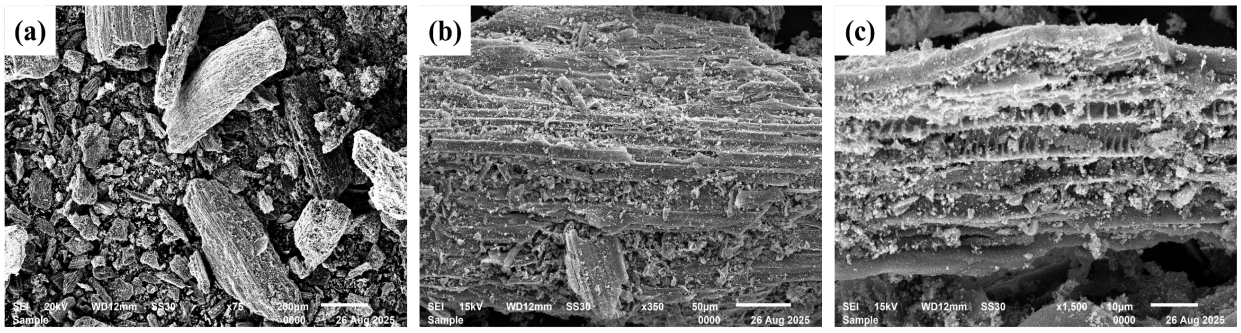


Figure 8. SEM of Graphitized biochar.

3.2.3 FTIR of graphitized biochar

The FTIR spectrum in Figure 9(a) shows observable chemical change in the graphitized biochar in comparison to the CH_retort. The FTIR spectrum of CH_retort has distinct peaks indicating presence of various functional groups whereas the FTIR spectrum of graphitized char is almost featureless, which is a clear indication of a highly ordered carbonaceous material such as graphite in which most of the functional groups have been eliminated.

CH_retort shows a broad band at around 3400 cm^{-1} indicating the O–H stretching whereas in graphitized char, this peak has almost disappeared. The high temperature treatment removes adsorbed water as well as decomposes hydroxyl-containing functional groups in retort biochar. Similarly, it also lacks aliphatic C–H stretches from methyl ($–CH_3$) and methylene ($–CH_2–$) groups as the aliphatic carbon chains are thermally cracked and eliminated during graphitization, leaving behind predominantly aromatic carbon structure. The oxygen functional groups are unstable at higher temperature and are removed as CO or CO_2 gases which is further indicated from the absence of carbonyl (C=O) or carboxyl groups (O–C=O) from esters, carboxylic acids, or ketones at around 1700 cm^{-1}. The peak at 1600 cm^{-1} owing to C=C stretch has become less intense and is present as a broad weak peak in graphitised char. This can be explained by the formation of larger, more continuous, and electrically conductive graphene sheets in the graphitisation process. Studies show that in perfect graphite the C=C stretch becomes very weak due to the high conductivity and symmetry of the crystal lattice. Thus, the almost disappearance of this peak is a direct indicator of successful graphitization. Fingerprint Region of CH_retort shows several distinct peaks in this region of 1100 cm^{-1} to 1300 cm^{-1} and 900 cm^{-1} to 700 cm^{-1} due to the presence of C–O stretches of alcohols, acids, esters and aromatic C–H out of plane bending respectively further revealing the substitution pattern in the aromatic rings. In contrast, in graphitized char reduced peaks of the "fingerprint region" confirms the reduced density of heteroatoms (O, H) further transforming it into a clean, polyaromatic carbon structure with high symmetry providing it close resemblance to graphite. This type of functional synthetic carbon material is suited for high-end applications such as energy storage devices (Li batteries, supercapacitors, fuel cells), environmental monitoring, and electro-chemical sensing [38]. Specifically, biochar shows promising potential as an anode material in Li–ion batteries, as metabolic modulator in anaerobic digestion [99]. These roles provide valuable insights for the engineering of valuable carbon materials to enhance waste to bio-energy recovery.

3.2.4 Raman spectroscopy of graphitized biochar

Raman spectroscopy provides insight into the char structure during graphitization process which occur at higher temperature. Raman spectra of graphitized char in Figure 9(b) represents defining features such as the intense and sharp G peak, the strong 2D peak and D peak, diagnostic of a material with exceptional structural quality. The sharp, intense peaks and their specific positions and shapes are definitive fingerprints of crystalline sp^2–carbon network with minimal disorder, which is indicative of synthetically produced, good quality graphitic material.

G Peak at approx. 1570 cm^{-1} is the hallmark of all graphitic carbon materials, attributed to in plane vibrational mode of sp^2 bonded carbon atoms. This most prominent peak in the spectrum with its highly intense sharp peak indicates a long-range crystalline order in the carbon lattice where atoms are vibrating in a highly uniform environment. The 2D Peak or G' Peak at 2675 cm^{-1}, a second order overtone of D band is the most sensitive indicators of graphene layers [63]. In this spectrum, 2D peak is very strong and well-defined as a result of iron mediated catalytic graphitization. This type of G band is typical of stacked graphene layers in highly ordered pyrolytic graphite [100]. Raman spectra of Graphitized carbon suggest the growth of graphite crystals and aromatic carbon clusters which further indicates that annealing facilitated by graphitization increases the structural order as sp^3 carbon atoms are transformed into sp^2 carbons along with H_2 gas effusion from the carbon-based material. During thermal annealing hydrogen atoms are removed, the intensity of D band increases as Fe mediated catalytic crosslinking forms sp^2 aromatic rings with improved order and thus promoting polymerization of carbon and further enhancement of graphitization degree. This indicates that the amorphous carbon has now transformed into a more ordered structure at high temperature [12]. At the same time the G band shifts to higher wavenumber. Raman spectrum as represented in Figure 9(b) is characteristic of a highly graphitized carbon material, such as graphene, highly ordered pyrolytic graphite or carbon material which is not a typical biochar spectrum. The previously analysed biochars (CH_550, CH_TLUD, CH_retort), exhibited disordered, amorphous carbon structure, whereas the Raman spectrum of graphitized biochar is indicative of a highly graphitized material which is evidenced by the 2D band. Thus, this graphitized carbon-based material represents the final stage of this thermal mediated structural evolution where the graphitic domains with fewer defects are stacked in layers. This kind of material is potentially suitable for advanced applications in electronics, composites, and energy storage [101].

3.2.5 XRD of graphitized biochar

Figure 10(a–b) displays the XRD analysis of commercial graphite and graphitized biochar respectively. The peaks in the graph represent intensity of the different planes in the graphite showing change in the crystalline structure. The diffraction peak in Figure 10(b) at 26.42° corresponds to graphitized carbon [102]. This peak can be indexed to the (002) plane spacing with (PDF no. 89–8487) diffraction of graphite [103]. The (002) peak of retort char shifted significantly post catalytic graphitization and the peak corresponding to the graphitic carbon in graphitized carbon was observed to be identical to that of the commercial graphite i.e. at 26.55°. Thus, it confirmed that the biochar was effectively graphitized due to the synergistic effect of heating along with mediation of metal catalyst involving heating and dissolution or precipitation during cooling process [104]. The broad peak at 43.62° with medium intensity in Figure 10(b) is due to (001) plane indicating presence of aromatic ring structures in the disordered or amorphous domain of graphitic carbon [63,105]. The (001) peak is said to be overlapped with the peak of Fe_3C (Iron carbide) indicating simultaneous graphitization and Fe_3C formation which is further confirmed from the HRTEM images showing dark inclusion in biochar [43]. Studies also reveal that in the given temperature window, conversion of amorphous carbon

is mainly aided by formation of Fe, which imply the structural evolution of amorphous carbon to mesoporous structures is closely associated with formation of Fe_3C [12].

3.3 Electrochemical response of biochar-based electrodes

The cyclic voltammogram is obtained for CH_retort biochar and metal oxide modified biochar (MO_retort) using 0.1 M phosphate buffer solution (pH 7.0) as supporting electrolyte in the presence as well as absence of paracetamol. It could be observed that in both CH_retort and MO_retort, the cyclic voltammograms recorded in the blank (only supporting electrolyte) did not present any redox peaks in the studies potential window as desired, shown in Figure 11(a–b). However, upon addition of 0.001M paracetamol into the electrolyte, well defined oxidation and reduction peaks emerged for both electrodes, thereby confirming successful electrocatalytic oxidation of paracetamol. This confirms that the observed electrochemical response arises exclusively from the oxidation of paracetamol rather than contributions from the electrolyte [106].

Figure 11(c) represents the cyclic voltammograms of CH_retort and MO_retort in presence of 0.001 M paracetamol in the electrolyte. CH_retort exhibits anodic and cathodic peak current of 1.820 mA and –1.195 mA respectively whereas MO_retort has anodic and cathodic peak current of 4.605 mA and –4.451 mA respectively. It could also be observed that the peak current in cyclic voltammogram is higher for MO_retort compared to CH_retort in presences of 0.001 M paracetamol, further indicating significant enhancement in electrocatalytic activity. This could be attributed to the higher electroactive surface area due to incorporation of metal oxide in MO_retort [107,108]. The improved electrochemical response is primarily due to synergistic interaction between biochar and catalytically active metal oxide which provides abundant active sites for efficient oxidation, thereby producing higher peak current [109]. The biochar can be further modified and studied for these kinds of electrochemical applications.

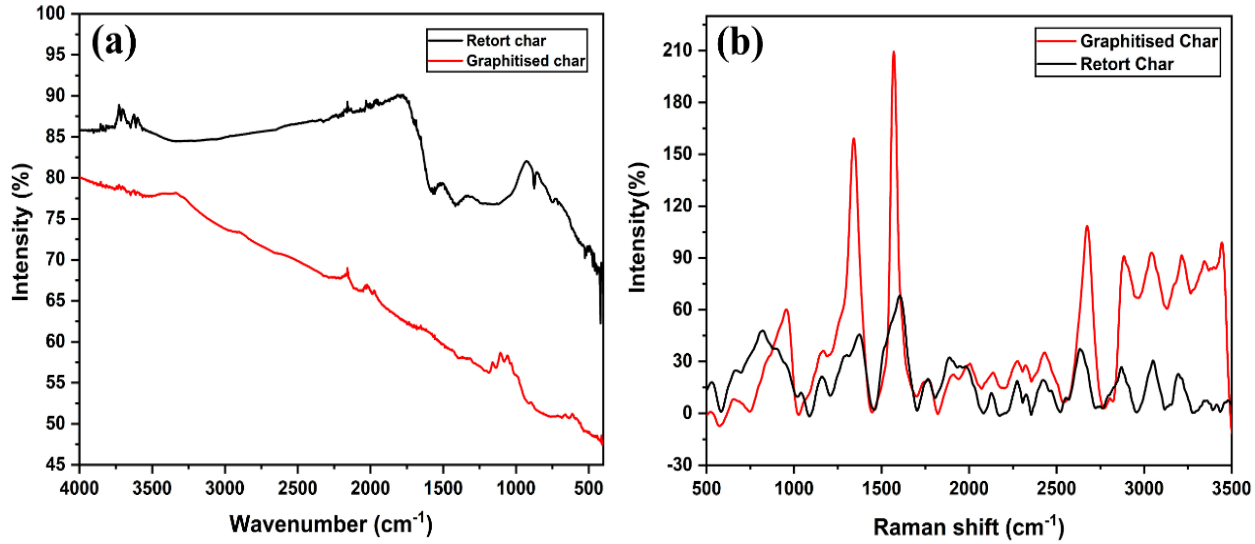


Figure 9. (a) FTIR of graphitized biochar, and (b) Raman of graphitized biochar.

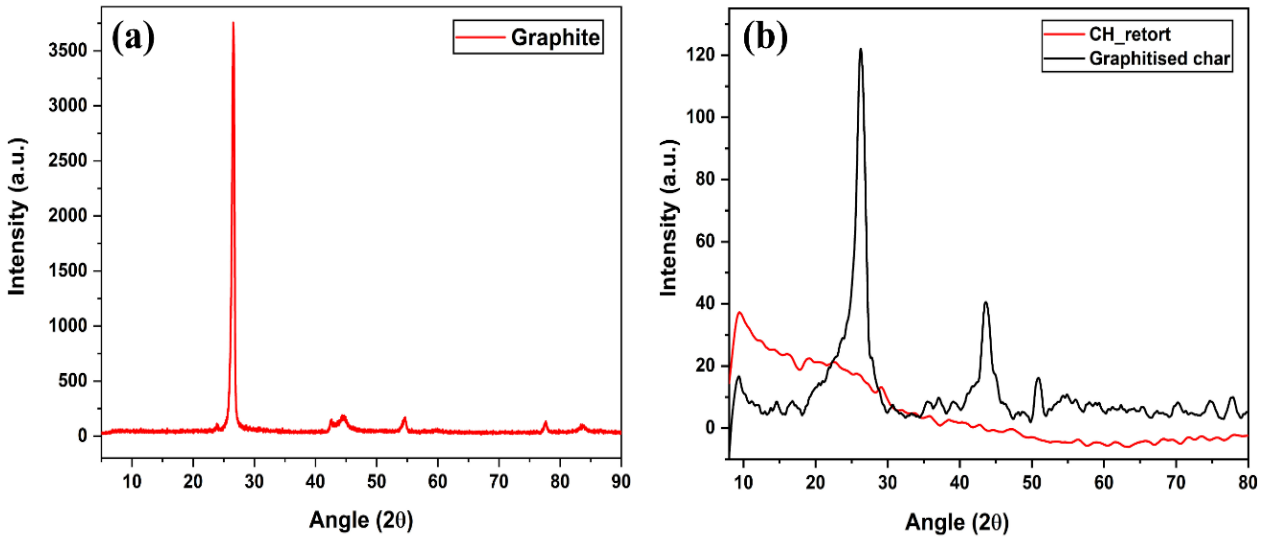


Figure 10. XRD of (a) graphite, and (b) graphitized biochar.

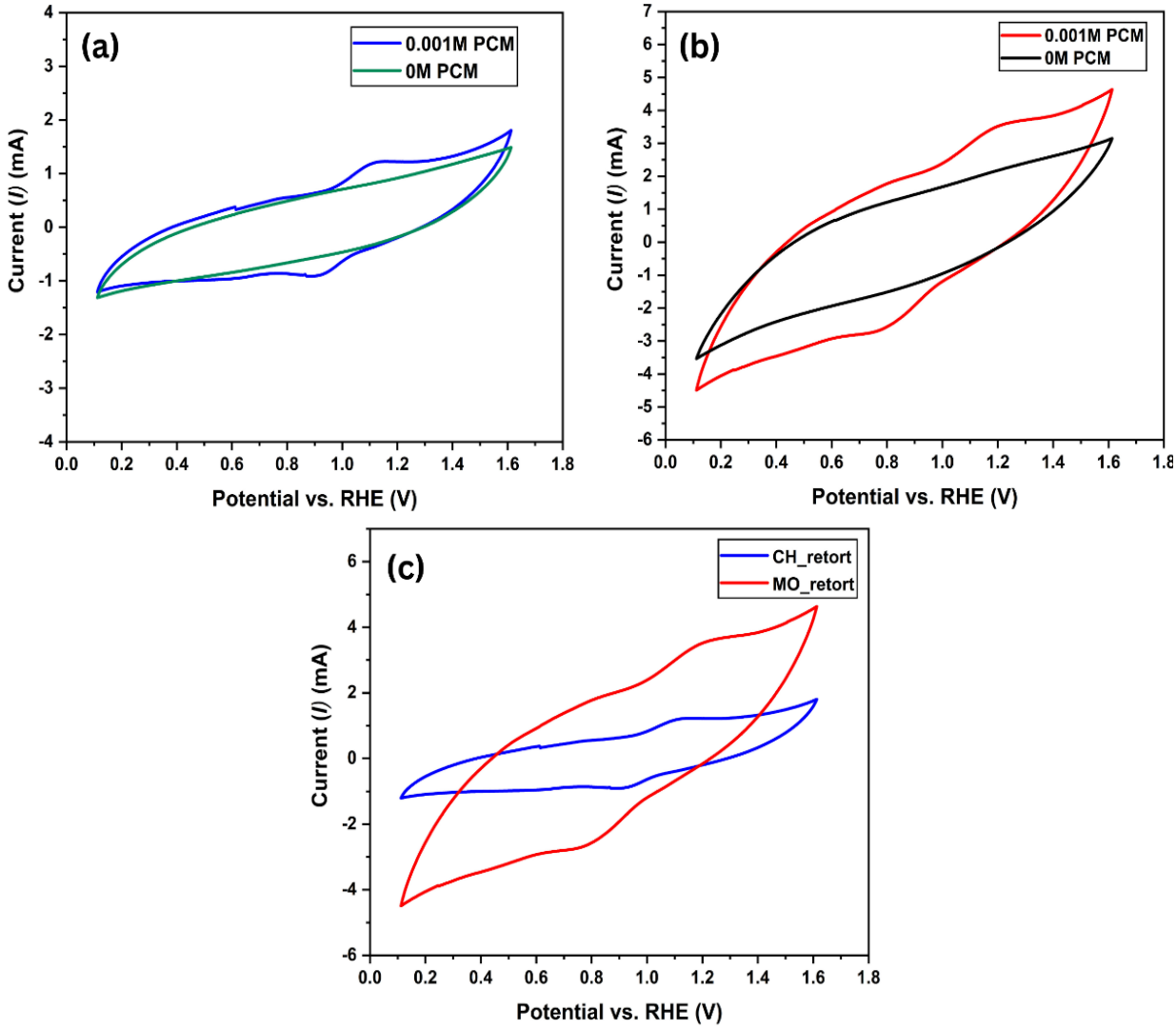


Figure 11. Cyclic voltammograms obtained in 0.1 M phosphate buffer solution (pH 7.0) in absence and presence of 0.001 M paracetamol (a) CH_retort, (b) MO_retort, and (c) Comparison of cyclic voltammograms of CH_retort and MO_retort in presence of 0.001 M paracetamol.

4. Conclusion

The present study illustrates the pine needle waste as a probable feedstock to produce biochar and biochar derived synthetic functional carbon nanomaterials. Attempt has been made to carbonize pine needles into biochar at different temperatures 300°C (CH_300), 400°C (CH_400), 550°C (CH_550) and 700°C (CH_700) through electric furnace method and in two small-scale biomass-kiln method named as Top Lit Updraft (CH_TLUD) and Retort kiln (CH_retort). The morphological, elemental and structural characteristics of all the prepared biochar samples were studied compared for their final characteristic features that defines the effect of temperature and highlights the difference between biochar prepared in furnace under inert atmosphere and the biochar produced through crude kiln heating method under restricted supply of oxygen. The biochar produced in electric furnace at 550°C and through retort kiln method exhibits promising results with good yield, carbon content >70%, and moderate polarity index polarity index [(O+N)/C]. FTIR, XRD, and Raman studies confirms the complete degradation of cellulose during charring process along with the formation and reorganization of aromatic domains. Furthermore, the biochar prepared by retort heating method is modified by metal oxide and is studied for its potential application as an electrode material for oxidation of paracetamol. The cyclic voltammogram indicates improved oxidation of paracetamol in the metal oxide modified biochar, which presents scope for future studies in this area.

Additionally, attempt has also been made to prepare graphitized carbon material using sustainable biochar through catalytic graphitization method at reduced temperature of 950°C. Characterization techniques including FTIR, Raman, XRD confirms successful synthesis of graphitic carbon material with a high degree of graphitization. Graphitized carbon material thus produced is a valuable material that can further be modified into graphene- based nanomaterials and can be utilized in advanced application in the field of electronics, energy storage (fuel cell, supercapacitor, anode material in Li batteries), wastewater treatment etc.

Thus, the concept of processing pine needle waste into biochar and biochar derived functional carbon materials provides an effective and sustainable pathway for waste to resource conversion that shows potential to meet high demand for commercial graphite-based materials in this energy era.

Data availability

All data generated or analysed during this study are included in this published article and its supplementary information files.

Declaration of competing interest

The authors declare that there is no conflict of interests regarding the publication of this paper.

Acknowledgements

This research study was financially supported by International Atomic Energy Agency (IAEA) Vienna, Austria (Award No.: 26450). The authors are thankful to Amity University, University Science Instrumentation centre (USIC), CRF IIT Delhi, Indian Institute of Science and University of Oulu for facilitating characterization support.

References

[1] R. Lesch, E. D. Visser, N. S. Seroka, and L. Khotseng, "Biomass-derived carbon-based nanomaterials: Current research, trends, and challenges," *Journal of Renewable Materials*, vol. 13, no. 10, pp. 1935–1977, 2025.

[2] J. Jiang, D. Deng, Y. Wang, Y. Chen, Y. Bai, M. Wang, X. Xiong, and Y. Lei, "Hydroxyl combined with nitrogen on biomass carbon promotes the electrocatalytic H_2O_2 selectivity," *Journal of Metals, Materials and Minerals*, vol. 35, no. 1, p. e2216, 2025.

[3] Q. Lin, R. Zhang, C. Yan, Q, Hu, S. Sang, Q. Wu, K. Liu, and H. Liu, "Regulating CoPx/Co heterostructures for enhanced electrocatalytic activity toward hydrazine oxidation reaction," *Journal of Metals, Materials and Minerals*, vol. 35, no. 2, p. e2348, 2025.

[4] K. Chaturvedi, A. Singhwane, M. Dhangar, M. Mill, N. Gorhae, A. Naik, P. Nair, A. K. Srivastava, and S. Verma, "Bamboo for producing charcoal and biochar for versatile applications," *Biomass Conversion and Biorefinery*, vol. 14, no. 14, pp. 15159–15185, 2024.

[5] R. Saidur, E. A. Abdelaziz, A. Demirbas, M. S. Hossain, and S. Mekhilef, "A review on biomass as a fuel for boilers," *Renewable and Sustainable Energy Reviews*, vol. 15, no. 5, pp. 2262–2289, 2011.

[6] D. MP, M. Misra, and A. K. Mohanty, "Recent advances on value-added biocarbon preparation by the pyrolysis of renewable and waste biomass, their structure and properties: A move toward an ecofriendly alternative to carbon black," *Environmental Science: Advances*, vol. 2, no. 10, pp. 1282–1301, 2023.

[7] M. Bartoli, R. Arrigo, G. Malucelli, A. Tagliaferro, and D. Duraccio, "Recent advances in biochar polymer composites," *Polymers (Basel)*, vol. 14, no. 12, p. 2506, 2022.

[8] T. A. T. Yasim-Anuar, L. Ng, A. A. Lawal, M. A. A. Farid, M. Yusuf, M. A. Hassan, and H. Ariffin, "Emerging application of biochar as a renewable and superior filler in polymer composites," *RSC Advances*, vol. 12, no. 22, pp. 13938–13949, 2022.

[9] M. Aboughaly, A. Babaei-Ghazvini, P. Dhar, R. Patel, and B. Acharya, "Enhancing the potential of polymer composites using biochar as a filler: A review," *Polymers (Basel)*, vol. 15, no. 19, p. 3981, 2023.

[10] A. Babich, and D. Senk, "Coal use in iron and steel metallurgy," in *The Coal Handbook: Towards Cleaner Production*, Elsevier, 2013, pp. 267–311.

[11] A. Lu, and J. Qin "A review on biomass-derived hard carbon anodes for sodium-ion batteries: From carbon precursors to storage mechanisms," *Journal of Metals, Materials and Minerals*, vol. 36, no. 1, p. e2555, 2026.

[12] Z. Sun, D. Yao, C. Cao, Z. Zhang, L. Zhang, H. Zhu, Q. Yuan, and B. Yi, "Preparation and formation mechanism of biomass-based graphite carbon catalyzed by iron nitrate under a low-temperature condition," *Journal of Environmental Management*, vol. 318, p. 115555, 2022.

[13] K. Plenča, S. Cvetnić, H. Prskalo, M. Kovacic, M. Cventnic, H. Kusic, Z. Matusinović, M. K. Rokovic, B. Genorio, U. L. Štangar, and A. L. Bozic, "Biomass pyrolysis-derived biochar: A versatile precursor for graphene synthesis," *Materials*, vol. 16, no. 24, p. 7658, 2023.

[14] H. You, J. Hui, Y. Zhou, K. Vittore, J. Zhang, L. E. Chaney, S. Chinta, Y. Zhao, G. Lim, D. Lee, E. A. Ainsworth, J. B. Dunn, V. P. Dravid, M. C. Hersam, and S. J. Rowan, "Sustainable production of biomass-derived graphite and graphene conductive inks from biochar," *Small*, vol. 20, no. 52, 2024.

[15] B. P. Chang, A. Rodriguez-Uribe, A. K. Mohanty, and M. Misra, "A comprehensive review of renewable and sustainable biosourced carbon through pyrolysis in biocomposites uses: Current development and future opportunity," *Renewable and Sustainable Energy Reviews*, vol. 152, p. 111666, .2021.

[16] Y. Li, R. Gupta, Q. Zhang, and S. You, "Review of biochar production via crop residue pyrolysis: Development and perspectives," *Bioresource Technology*, vol. 369, p. 128423, 2023.

[17] A. M. Zubairu, E. Micheli, C. M. Ocensey, N. Boros, G. Rethati, E. Lehoczky, and M. Gulyas, "Biochar improves soil fertility and crop performance: A case study of Nigeria," *Soil Systems*, vol. 7, no. 4, p. 105, 2023,

[18] M. Obonukut, S. Alabi, and A. Jock, "Biochar from cassava waste: A paradigm shift from waste to wealth," in *Biochar-Productive Technologies, Properties and Applications*, Intech Open, 2023.

[19] W. Buss, C. Wurzer, D. A. C. Manning, E. J. Rohling, J. Borevitz, and O. Mašek, "Mineral-enriched biochar delivers enhanced nutrient recovery and carbon dioxide removal," *Communications Earth & Environment*, vol. 3, no. 1, p. 67, 2022.

[20] D. A. E. L. André Brunnberg, "Catalytic graphitization of biomass," Kth Royal Institute of Technology School of Industrial Engineering And Management, 2021.

[21] M. Fayazi, "Synthesis of ZnO nanostructures with different morphologies on biochar support for photocatalytic degradation of organic dye," *Journal of Water and Environmental Nanotechnology*, 2024.

[22] L. Rodrigues, A. Budai, L. Elsgaard, B. Hardy, S. G. Keel, C. Mondini, C. Plaza, and J. Leifeld, "The importance of biochar quality and pyrolysis yield for soil carbon sequestration in

practice," *European Journal of Soil Science*, vol. 74, no. 4, 2023,

[23] M. I. Awad, Y. Makkawi, and N. M. Hassan, "Yield and energy modeling for biochar and bio-oil using pyrolysis temperature and biomass constituents," *ACS Omega*, vol. 9, no. 16, pp. 18654–18667, 2024.

[24] G. Stella Mary, P. Sugumaran, S. Niveditha, B. Ramalakshmi, P. Ravichandran, and S. Seshadri, "Production, characterization and evaluation of biochar from pod (Pisum sativum), leaf (Brassica oleracea) and peel (Citrus sinensis) wastes," *International Journal of Recycling of Organic Waste in Agriculture*, vol. 5, no. 1, pp. 43–53, 2016.

[25] R. Wood, O. Mašek, and V. Erastova, "Developing realistic molecular models of biochars," *Cell Reports Physical Science*, vol. 5, no. 7, p. 102037, 2024.

[26] K. A. Spokas, "Review of the stability of biochar in soils: predictability of O:C molar ratios," *Carbon Manag.*, vol. 1, no. 2, pp. 289–303, 2010.

[27] D. Krügerm, and Ö. Ç. Mutlu, "Demonstration of a top-lit updraft based pyrolytic burner with low emission operation and automatic process control," *Energies (Basel).*, vol. 14, no. 13, p. 3913, 2021.

[28] J. Sánchez-Pólito, V. Berrueta; V. Ruiz-García; A. Beltrán; E. Herrera-Medina; M. Cazarez-Barboza; L. lvarez-Icaza; and O. Masera "Development and evaluation performance of top-lit updraft biomass micro-gasifiers for energy-intensive household cooking tasks in Mexico," *Sustainable Energy Technologies and Assessments*, vol. 67, p. 103813, 2024,

[29] J. O. Ighalo, O. A. A. Eletta, and A. G. Adeniyi, "Biomass carbonisation in retort kilns: Process techniques, product quality and future perspectives," *Bioresource Technology Reports*, vol. 17, p. 100934, 2022.

[30] A. Chandrasekaran, S. Subbiah, S. Ramachandran, S. Narayanasamy, P. Bartocci, and F. Fantozzi, "Natural draft-improved carbonization retort system for biocarbon production from *prosopis juliflora* biomass," *Energy & Fuels*, vol. 33, no. 11, pp. 11113–11124, 2019.

[31] T. Namaswa, D. F. R. P. Burslem, and J. Smith, "Emerging trends in appropriate kiln designs for small-scale biochar production in low to middle income countries," *Bioresource Technology Reports*, vol. 24, p. 101641, 2023.

[32] T. J. Bandosz, "Surface chemistry of carbon materials," in *Carbon Materials for Catalysis*, Wiley, 2008, pp. 45–92.

[33] B.-T. T. Dao, D. T. Nguyen, N. H. Le, and C.-N. Ha-Thuc, "Synergistic adsorption–photocatalysis of activated carbon/titanium dioxide composite derived from rice husk ash under ultraviolet-C irradiation," *Journal of Metals, Materials and Minerals*, vol. 36, no. 3, p. e2597, 2026.

[34] J. Wang, Z. Li, Y. Li, Z. Wang, X. Liu, Z. Liu, and J. Ma, "Evolution and correlation of the physiochemical properties of bamboo char under successive pyrolysis process," *Biochar*, vol. 6, no. 1, p. 33, 2024.

[35] G. Loebsack, K. K.-C. Yeung, F. Berruti, and N. B. Klinghoffer, "Impact of biochar physical properties on adsorption mechanisms for removal of aromatic aqueous contaminants in water," *Biomass Bioenergy*, vol. 194, p. 107617, 2025.

[36] R. Kumar, P. K. Rakesh, and D. Sreehari, "Investigation on physico-chemical, mechanical and thermal properties of extracted novel pinus roxburghii fiber," *Journal of Natural Fibers*, vol. 20, no. 1, 2023.

[37] I. Pavkov, M. Radojcin, Z. Stamenkovic, S. Bikic, M. Tomic, M. Bukurov, and B. Despotovic, "Hydrothermal carbonization of agricultural biomass: characterization of hydrochar for energy production," *Solid Fuel Chemistry*, vol. 56, no. 3, pp. 225–235, 2022.

[38] S. Shyam, M. Daimary, M. Narayan, and H. Sarma, "Biochar-based electroanalytical materials: Towards sustainable, high-performance electrocatalysts and sensors," *Next Materials*, vol. 8, p. 100873, 2025.

[39] I. Cakin, S. Pap, P. P. J. Gaffney, and M. A. Taggart, "Designing a biochar-based pretreatment method for distillery effluents entering constructed wetlands," *The Journal of Cleaner Production*, vol. 476, p. 143790, 2024.

[40] P. Bulak, K. Proc-Pietrycha, M. Kaczor, K. Zlotko, C. Polakowski, D. Wiacek, H. Waniak-Nawicka, E. Zieba, A. Wasko, P. Oleszczuk, and A. Bieganowski, "A novel type of biochar from chitinous Hermetia illucens waste with a built-in stimulating effect on plants and soil arthropods," *Scientific Reports.*, vol. 13, no. 1, p. 8306, 2023,

[41] M. A. Islam, M. I. Parvin, T. K. Dada, R. Kumar, and E. Antunes, "Silver adsorption on biochar produced from spent coffee grounds: validation by kinetic and isothermal modelling," *Biomass Conversion and Biorefinery*, vol. 14, no. 22, pp. 28007–28021, 2024.

[42] R. Breen, C. Goggin, J. D. Holmes, and G. Collins, "A collaborative cocurricular undergraduate research experience on sustainable materials: Analysis of biochar using the boehm titration and spectroscopic techniques," *Journal of Chemical Education*, vol. 102, no. 3, pp. 1323–1332, 2025.

[43] C. Wang, D. Ma, and X. Bao, "Transformation of biomass into porous graphitic carbon nanostructures by microwave irradiation," *The Journal of Physical Chemistry C*, vol. 112, no. 45, pp. 17596–17602, 2008.

[44] X. Yang, H. Pan, S. M. Shaheen, H. Wang, and J. Rinklebe, "Immobilization of cadmium and lead using phosphorus-rich animal-derived and iron-modified plant-derived biochars under dynamic redox conditions in a paddy soil," *Environment International*, vol. 156, p. 106628, 2021.

[45] A. Kumar, S. D. Joseph, E. R. Graber, S. Tahery, D. R. G. Mitchell, P. Munroe, L. Tsechansky, O. lerdahl, W. Aker, and M. Saebo, "Fertilizing behavior of extract of organomineral-activated biochar: Low-dose foliar application for promoting lettuce growth," *Chemical and Biological Technologies in Agriculture*, vol. 8, no. 1, p. 21, 2021.

[46] R. Chatterjee, B. Sajjadi, W.-Y. Chen, D. Mattern, N. Hammer, V. Raman, and A. L. Dorris, "Effect of pyrolysis temperature on physicochemical properties and acoustic-based amination of biochar for efficient CO_2 adsorption," *Frontiers in Energy Research*, vol. 8, 2020.

[47] Y. Cui, X. Chen, C. Pitakrattanawong, X. Du, L. Qiu, H. Xu, J. Chen, M. Shunlong, L. Fan, and S. Chao, "Adsorption efficiency of biochar produced by aquaculture by-products for removing

geosmin in aquaculture environment," *Water Reuse*, vol. 14, no. 1, pp. 65–79, 2024.

[48] S. S. Sahoo, V. K. Vijay, R. Chandra, and H. Kumar, "Production and characterization of biochar produced from slow pyrolysis of pigeon pea stalk and bamboo," *Cleaner Engineering and Technology,* vol. 3, p. 100101, 2021.

[49] R. Liu, G. Liu, B. Yousaf, Z. Niu, and Q. Abbas, "Novel investigation of pyrolysis mechanisms and kinetics for functional groups in biomass matrix," *Renewable and Sustainable Energy Reviews*, vol. 153, p. 111761, 2022.

[50] E. M. El-Fawal, A. M. A. El-Naggar, A. A. El-Zahhar, M. M. Alghandi, A. Morshedy, H. A. El-Sayed, an A. E. M. Mohammed, "Biofuel production from waste residuals: comprehensive insights into biomass conversion technologies and engineered biochar applications," *RSC Advances*, vol. 15, no. 15, pp. 11942–11974, 2025.

[51] W. Suliman, J. B. Harsh, N. I. Abu-Lail, A.-M. Fortuna, I. Dallmeyer, and M. Garcia-Pérez, "The role of biochar porosity and surface functionality in augmenting hydrologic properties of a sandy soil," *Science of The Total Environment*, vol. 574, pp. 139–147, 2017.

[52] S. V. Vongsetskul, W. Thepthong, S. Kanyawilas, N. Chanlek, R. Charoenwattanasatien, W. Busayaporn, T. Vongsetskul, "Zinc oxide functionalized biochar from rambutan wood as a novel material to utilize an agricultural waste in Thailand," *Journal of Metals, Materials and Minerals*, vol. 36, no. 2, p. e2410, 2026.

[53] Q. Luo, Y. Deng, Y. Li, Q. He, H. Wu, and X. Fang, "Effects of pyrolysis temperatures on the structural properties of straw biochar and its adsorption of tris-(1-chloro-2-propyl) phosphate," *Scientific Reports.*, vol. 14, no. 1, p. 25711, 2024.

[54] A. K. Varma, and P. Mondal, "Physicochemical characterization and kinetic study of pine needle for pyrolysis process," *Journal of Thermal Analysis and Calorimetry*, vol. 124, no. 1, pp. 487–497, 2016.

[55] A. K. Varma, and P. Mondal, "Pyrolysis of pine needles: effects of process parameters on products yield and analysis of products," *Journal of Thermal Analysis and Calorimetry*, vol. 131, no. 3, pp. 2057–2072, 2018.

[56] A. Tomczyk, Z. Sokołowska, and P. Boguta, "Biochar physicochemical properties: pyrolysis temperature and feedstock kind effects," *Reviews in Environmental Science and Bio/Technology*, vol. 19, no. 1, pp. 191–215, 2020.

[57] M. Ahmad, S. S. Lee, A. U. Rajapaksha, M. Vithanage, M. Zhang, J. S. Cho, S. E. Lee, and Y. S. Ok, "Trichloroethylene adsorption by pine needle biochars produced at various pyrolysis temperatures," *Bioresource Technology*, vol. 143, pp. 615–622, 2013.

[58] C. Zhang, N. Zhang, Z. Xiao, Z. Li, and D. Zhang, "Characterization of biochars derived from different materials and their effects on microbial dechlorination of pentachlorophenol in a consortium," *RSC Advances*, vol. 9, no. 2, pp. 917–923, 2019.

[59] M. Keiluweit, P. S. Nico, M. G. Johnson, and M. Kleber, "Dynamic molecular structure of plant biomass-derived black carbon (biochar)," *Environmental Science & Technology*, vol. 44, no. 4, pp. 1247–1253, 2010.

[60] S. Malik, and J. S. Laura, "Evaluating biochar properties derived from various agro-residues via pyrolysis: A comparative study," *Oriental Journal of Chemistry*, vol. 41, no. 1, pp. 120–126, 2025.

[61] S. Jha, R. Gaur, S. Shahabuddin, I. Tyagi, J. Giri, and M. Kanan, "Utilizing low-cost mausambi peel-derived adsorbents for the effective treatment of complex industrial dye mixture in wastewater: Unravelling the adsorption mechanism," *Cleaner Engineering and Technology*, vol. 26, p. 100951, 2025.

[62] H. Darmstadt, D. Pantea, L. Sümmchen, U. Roland, S. Kaliaguine, and C. Roy, "Surface and bulk chemistry of charcoal obtained by vacuum pyrolysis of bark: influence of feedstock moisture content," *Journal of Analytical and Applied Pyrolysis*, vol. 53, no. 1, pp. 1–17, 2000.

[63] C. Schneider, S. Walker, A. Phounglamcheik, K. Umeki, and T. Kolb, "Effect of calcium dispersion and graphitization during high-temperature pyrolysis of beech wood char on the gasification rate with CO_2," *Fuel*, vol. 283, p. 118826, 2021.

[64] N. Kumari, T. Chhabra, S. Kumar, and V. Krishnan, "Nano-architectonics of sulfonated biochar from pine needles as catalyst for conversion of biomass derived chemicals to value added products," *Catalysis Communications*, vol. 168, p. 106467, 2022.

[65] R. K. Gond, M. K. Gupta, H. Singh, S. Mavinkere Rangappa, and S. Siengchin, "Extraction and properties of cellulose for polymer composites," in *Biodegradable Polymers, Blends and Composites*, Elsevier, 2022, pp. 59–86.

[66] S. Yoo, S. S. Kelley, D. C. Tilotta, and S. Park, "Structural characterization of loblolly pine derived biochar by X-ray diffraction and electron energy loss spectroscopy," *ACS Sustainable Chemistry & Engineering*, vol. 6, no. 2, pp. 2621–2629, 2018.

[67] S. Biswas, H. Siddiqi, B. C. Meikap, T. K. Sen, and M. Khiadani, "Preparation and characterization of raw and inorganic acid-activated pine cone biochar and its application in the removal of aqueous-phase Pb^{2+} metal ions by adsorption," *Water, Air, & Soil Pollution*, vol. 231, no. 1, p. 3, 2020.

[68] O. Paris, C. Zollfrank, and G. A. Zickler, "Decomposition and carbonisation of wood biopolymers—a microstructural study of softwood pyrolysis," *Carbon N. Y.*, vol. 43, no. 1, pp. 53–66, 2005.

[69] P. Nain, "Characterization of pine needle and pine needle biochar: A potential soil amendment for sustainable forest waste management," *Annals of Plant and Soil Research*, vol. 25, no. 2, pp. 211–220, 2023.

[70] T. Yang, and A. C. Lua, "Characteristics of activated carbons prepared from pistachio-nut shells by physical activation," *Journal of Colloid and Interface Science*, vol. 267, no. 2, pp. 408–417, 2003.

[71] J. Zhang, B. Huang, L. Chen, J. Du, W. Li, and Z. Luo, "Pyrolysis kinetics of hulless barley straw using the distributed activation energy model (daem) by the TG/DTA technique and sem/xrd characterizations for hulless barley straw derived biochar," *Brazilian Journal of Chemical Engineering*, vol. 35, no. 3, pp. 1039–1050, 2018.

[72] J. Dias, A. Conceição, F. M. Delatorre, and P. Siqueira, "Production, characterization physical, chemical, and structural analysis of biochar fines for bio-reinforcement in composite materials," *Processes*, vol. 13, no. 2, p. 504, 2025.

[73] L. Xu, Q. Yao, J. Deng, Z. Han, Y. Zhang, Y. Fu, G. W. Huber, and Q. Guo, "Renewable N-heterocycles production by thermo-catalytic conversion and ammonization of biomass over ZSM-5," *ACS Sustainable Chemistry & Engineering*, vol. 3, no. 11, pp. 2890–2899, 2015.

[74] A. Rachmat, Y. E. Wahyu, P. L. Hariani, F. Riyanti, and F. Fatma, "Pyrolysis and modification of coconut shell into sulfonated biochar and its catalytic activity on cellobiose conversion," *Journal of Metals, Materials and Minerals*, vol. 35, no. 3, p. e2271, 2025.

[75] N. T. Abdel-Ghani, G. A. El-Chaghaby, and E. M. Zahran, "Cost effective adsorption of aluminium and iron from synthetic and real wastewater by rice hull activated carbon (RHAC)," *American Journal of Analytical Chemistry*, vol. 06, no. 01, pp. 71–83, 2015.

[76] S. O. Amusat, T. G. Kebede, E. N. Nxumalo, S. Dube, and M. M. Nindi, "Green synthesis of surface modified biochar for simultaneous removal of steroidal hormones and heavy metals from wastewater: Optimisation by central composite design," *Water (Basel)*, vol. 15, no. 20, p. 3703, 2023.

[77] B. Armynah, Atika, Z. Djafar, W. H. Piarah, and D. Tahir, "Analysis of chemical and physical properties of biochar from rice husk biomass," *Journal of Physics: Conference Series*, vol. 979, p. 012038, 2018.

[78] A. Illankoon, C. Milanese, A. Karunarathna, Y. Alanhakoon, P. G. Rathnasiri, M. Medina-Llamas, M. C. Collivignarelli, and S. Sorlini, "Development of a dual-chamber pyrolizer for biochar production from agricultural waste in sri lanka," *Energies (Basel)*, vol. 16, no. 4, p. 1819, 2023.

[79] M. Keiluweit, and M. Kleber, "Molecular-level interactions in soils and sediments: The role of aromatic π-systems," *Environmental Science & Technology* vol. 43, no. 10, pp. 3421–3429, 2009.

[80] V. Choudhary, M. Patel, C. U. Pittman, and D. Mohan, "Batch and continuous fixed-bed lead removal using himalayan pine needle biochar: Isotherm and kinetic studies," *ACS Omega*, vol. 5, no. 27, pp. 16366–16378, 2020.

[81] R. A. Mensah, V. Shanmugam, E. Kaynak, D. Sokol, J. Wahl, K. C. Le, Y. Zhang, L. Jiang, R. E. Neisiany, E. A. Turhan, and O. Das, "The facile conversion of waste biomass into few-layer graphene oxide," *Scientific Reports*, vol. 15, no. 1, p. 9166, 2025.

[82] D. Mohan, A. Sarswat, V. K. Singh, M. Alexandre-Franco, and C. U. Pittman, "Development of magnetic activated carbon from almond shells for trinitrophenol removal from water," *Chemical Engineering Journal*, vol. 172, no. 2–3, pp. 1111–1125, 2011.

[83] A. Ngambia, O. Mašek, and V. Erastova, "Development of biochar molecular models with controlled porosity," *Biomass Bioenergy*, vol. 184, p. 107199, 2024.

[84] M. Bin Mobarak, N. S. Pinky, S. Mustafi, F. Chowdhury, A. Nahar, U. S. Akhtar, Md. S. Quddus, S. Yasmin, and Md. A. Alam "Unveiling the reactor effect: a comprehensive characterization of biochar derived from rubber seed shell *via* pyrolysis and in-house reactor," *RSC Advances*, vol. 14, no. 41, pp. 29848–29859, 2024.

[85] S. Ekman, G. S. dos Reis, E. Laisne, J. Thivet, A. Grimm, E. C. Lima, Mu. Naushad, and G. Dotto, "Synthesis, characterization, and adsorption properties of nitrogen-doped nanoporous biochar: efficient removal of reactive orange 16 dye and colorful effluents," *Nanomaterials*, vol. 13, no. 14, p. 2045, 2023.

[86] Q. Lin, J. Zhang, L. Yin, H. Liu, W. Zuo, and Y. Tian, "Relationship between heavy metal consolidation and H_2S removal by biochar from microwave pyrolysis of municipal sludge: Effect and mechanism," *Environmental Science and Pollution Research*, vol. 28, no. 22, pp. 27694–27702, 2021.

[87] Z. Yao, X. Chen, Y. Sun, and W. Qi, "Simultaneous regulation of nitrogen, sulfur and carbon using biochar during sewage sludge pyrolysis," *ReNew Energy Global*, vol. 236, p. 121413, 2024.

[88] Z. Chen, W. Chen, D. Jia, Y. Liu, A. Zhang, T. Wen, J. Liu, Y. Ai, W. Song, and X. Wang, "N, P, and S codoped graphene-like carbon nanosheets for ultrafast uranium (VI) capture with high capacity," *Advanced Science*, vol. 5, no. 10, 2018.

[89] S. Oswald, M. V. Gorbunov, and D. Mikhailova, "Electron spectroscopy investigations of potassium and potassium-intercalated graphite with battery background," *Applied Surface Science* vol. 655, p. 159614, 2024.

[90] L. Cizaire, J. M. Martin, T. Le Mogne, and E. Gresser, "Chemical analysis of overbased calcium sulfonate detergents by coupling XPS, ToF-SIMS, XANES, and EFTEM," *Colloids and Surfaces A: Physicochemical and Engineering Aspects*, vol. 238, no. 1–3, pp. 151–158, 2004.

[91] S. Li, X. Liu, R. Mao, Z. Huang, and R. Xie, "Red-emission enhancement of the $CaAlSiN_3:Eu^{2+}$ phosphor by partial substitution for Ca_3N_2 by $CaCO_3$ and excess calcium source addition," *RSC Advances*, vol. 5, no. 93, pp. 76507–76515, 2015.

[92] T. K. Mandal, Y. Hou, Z. Gao, H. Ning, W. Yang, and M. Gao, "Graphene oxide-based sensor for ultrasensitive visual detection of fluoride," *Advanced Science*, vol. 3, no. 12, 2016.

[93] K. Suzuki, Y. Saito, N. Okazaki, and T. Suzuki, "Graphite-shell-chains selectively and efficiently produced from biomass rich in cellulose and chitin," *Scientific Reports*, vol. 10, no. 1, p. 12131, 2020.

[94] S. J. Goldie, and K. S. Coleman, "Graphitization by metal particles," *ACS Omega*, vol. 8, no. 3, pp. 3278–3285, 2023.

[95] S. G. Krishnan, C. E. White, K. Zeng, N. Kalarikkal, Y. S. Ok, C. B. Arnold, S. Thomas, and A. Nzihou "Recent developments on multi- versus single-metallic catalytic graphitisation of biocarbon: A review," *Fuel*, vol. 396, p. 135330, 2025.

[96] Z. Sun, D. Yao, C. Cao, Z. Zhang, L. Zhang, H. Zhu, Q. Yuan, and B. Yi "Preparation and formation mechanism of biomass-based graphite carbon catalyzed by iron nitrate under a low-temperature condition," *Journal of Environmental Management*, vol. 318, p. 115555, 2022.

[97] A. Gomez-Martin, Z. Schnepp, and J. Ramirez-Rico, "Structural evolution in iron-catalyzed graphitization of hard carbons," *Chemistry of Materials*, vol. 33, no. 9, pp. 3087–3097, 2021.

[98] S. M. Alluqmani, H. Albuqawi, M. A. Hakami, N. M. Alabdallah, H. M. Almarri, A. A. Al-Zahrani, and A. Alshahrie, "Preparation and characterisation of graphitic biochar materials derived from rose oil industry waste via different pyrolysis durations and

ball milling for advanced composites," *Materials Research Express*, vol. 11, no. 3, p. 035005, 2024.

[99] C. Yang, Z. Liu, W. Liu, Y. Qiu, S. Zhang, X. Zhang, M. Wang, H. Wu, L. Hongyi, J. Huang, J. Liu, Y. Wang, S. He, D. Gu, G. Xiaohui, X. Yang, T. Xie, H. Chen, and Y. Yao, "Graphitized biochar derived from agricultural wastes enhances methanogenesis via conductivity-driven direct interspecies electron transfer," *Advanced Science*, vol. 12, no. 41, 2025.

[100] I. Major, J.-M. Pin, E. Behazin, A. Rodriguez-Uribe, M. Misra, and A. Mohanty, "Graphitization of *Miscanthus* grass biocarbon enhanced by *in situ* generated FeCo nanoparticles," *Green Chemistry*, vol. 20, no. 10, pp. 2269–2278, 2018.

[101] T. Mazon, B. A. Bregadiolli, J. V. Paulin, W. A. Bizzo, L. T. Kubota, and S. Deng, "Application of graphitized sugarcane biochar and derivative composites as electrodes in supercapacitors," *SSRN Electronic Journal*, 2022.

[102] T. Kim, J. Lee, and K.-H. Lee, "Full graphitization of amorphous carbon by microwave heating," *RSC Advances*, vol. 6, no. 29, pp. 24667–24674, 2016.

[103] H. Li, Y. Xiao, X. Tian, X. Xing, M. Cao, and Y. Wang, "A crystalline/amorphous FeCo alloy/FeCoNi-Pi bifunctional electrocatalyst for efficient overall water splitting," *Inorganic Chemistry Frontiers*, vol. 11, no. 12, pp. 3585–3595, 2024.

[104] S. Khoshk Rish, A. Tahmasebi, R. Wang, J. Dou, and J. Yu, "Formation mechanism of nano graphitic structures during microwave catalytic graphitization of activated carbon," *Diamond and Related Materials*, vol. 120, p. 108699, 2021.

[105] T. Li, R. Ma, X. Xu, S. Sun, and J. Lin, "Microwave-induced preparation of porous graphene nanosheets derived from biomass for supercapacitors," *Microporous and Mesoporous Materials*, vol. 324, p. 111277, 2021.

[106] N. C. Silva de Souza, G. A. Puiatti, G. do C. Dias, R. M. Silva, R. P. Lopes Moreira, and T. A. Silva, "Development of sustainable electrodes based on cobalt ferrite-decorated biochar for the voltammetric determination of paracetamol in biological fluids," *Analytical Methods*, vol. 17, no. 17, pp. 3509–3516, 2025.

[107] Md. M. Rahman, A. Al Mamun, H. Minami, Md. M. Rahman, S. M. Hoque, and H. Ahmad, "Biochar/poly(aniline-pyrrole) modified graphite electrode and electrochemical behavior for application in low-cost supercapacitor," *Arabian Journal of Chemistry*, vol. 17, no. 9, p. 105938, 2024.

[108] H. Jing, D. Zheng, H. Du, H. Zhu, M. Chen, and Y. Zhou, "Cage-like ulva biochar confined synthesis of Fe_3O_4/ZnO heterojunction nanoparticles for synergistic adsorption and photocatalytic degradation of PFOA," *Biochar*, vol. 8, no. 1, p. 11, 2026.

[109] C. Mabrouk, J. Wannassi, P. A. Salazar-Carballo, S. Carinelli, A. J. Gross, H. Kahri, N. Jaffrezic-Renault, and H. Barhoumi "ZnO nanoparticles coated with EDTA and Ag nanoparticles (ZnO@EDTA-Ag NPs) for enhanced electrochemical detection of Cu^{2+} ions in food and environmental samples," *Microchemical Journal*, vol. 212, p. 113562, 2025.